nature chemical biology

Article

https://doi.org/10.1038/s41589-022-01154-9

Hepatic glutamine synthetase controls N^5-methylglutamine in homeostasis and cancer

Received: 18 February 2022

Accepted: 31 August 2022

Published online: 24 October 2022

Check for updates

Victor H. Villar[1], Maria Francesca Allega[1,2,8], Ruhi Deshmukh[1,8], Tobias Ackermann[1], Mark A. Nakasone[1], Johan Vande Voorde[1], Thomas M. Drake[1,2,3], Janina Oetjen[4], Algernon Bloom[2], Colin Nixon[1], Miryam Müller[1], Stephanie May[1], Ee Hong Tan[1], Lars Vereecke[5,6], Maude Jans[5,6], Gillian Blancke[5,6], Daniel J. Murphy[1,2], Danny T. Huang[1,2], David Y. Lewis[1,2], Thomas G. Bird[1,2,7], Owen J. Sansom[1,2], Karen Blyth[1,2], David Sumpton[1] and Saverio Tardito[1,2] ✉

Glutamine synthetase (GS) activity is conserved from prokaryotes to humans, where the ATP-dependent production of glutamine from glutamate and ammonia is essential for neurotransmission and ammonia detoxification. Here, we show that mammalian GS uses glutamate and methylamine to produce a methylated glutamine analog, N^5-methylglutamine. Untargeted metabolomics revealed that liver-specific GS deletion and its pharmacological inhibition in mice suppress hepatic and circulating levels of N^5-methylglutamine. This alternative activity of GS was confirmed in human recombinant enzyme and cells, where a pathogenic mutation in the active site (R324C) promoted the synthesis of N^5-methylglutamine over glutamine. N^5-Methylglutamine is detected in the circulation, and its levels are sustained by the microbiome, as demonstrated by using germ-free mice. Finally, we show that urine levels of N^5-methylglutamine correlate with tumor burden and GS expression in a β-catenin-driven model of liver cancer, highlighting the translational potential of this uncharacterized metabolite.

Glutamine is a non-essential amino acid in mammals that is exclusively synthesized by the enzyme glutamine synthetase (GS)[1]. Despite having been isolated from mammalian tissue more than 70 years ago[2], the pathophysiological role of GS has not been fully elucidated, and novel functions have recently been described in endothelium and macrophage biology[3,4]. Consistent with the role of glutamate and glutamine in neurotransmission[5] and neurodevelopment[6], inactivating point mutations in the GS active site cause severe neurodevelopmental defects that can cause perinatal death in humans[7].

One of the many metabolic functions of the liver is to detoxify the ammonia released into the systemic circulation by metabolic processes. Liver failure causes an increase in the concentration of ammonia

[1]Cancer Research UK Beatson Institute, Garscube Estate, Glasgow, UK. [2]Institute of Cancer Sciences, University of Glasgow, Glasgow, UK. [3]Department of Clinical Surgery, University of Edinburgh, Edinburgh, UK. [4]Bruker Daltonics GmbH & Co. KG, Bremen, Germany. [5]Host–Microbiota Interaction Lab, VIB Center for Inflammation Research, Ghent, Belgium. [6]Department of Internal Medicine and Pediatrics, Ghent University, Ghent, Belgium. [7]Centre for Inflammation Research, The Queen's Medical Research Institute, University of Edinburgh, Edinburgh, UK. [8]These authors contributed equally: Maria Francesca Allega, Ruhi Deshmukh. ✉e-mail: s.tardito@beatson.gla.ac.uk

https://doi.org/10.1038/s41589-022-01154-9

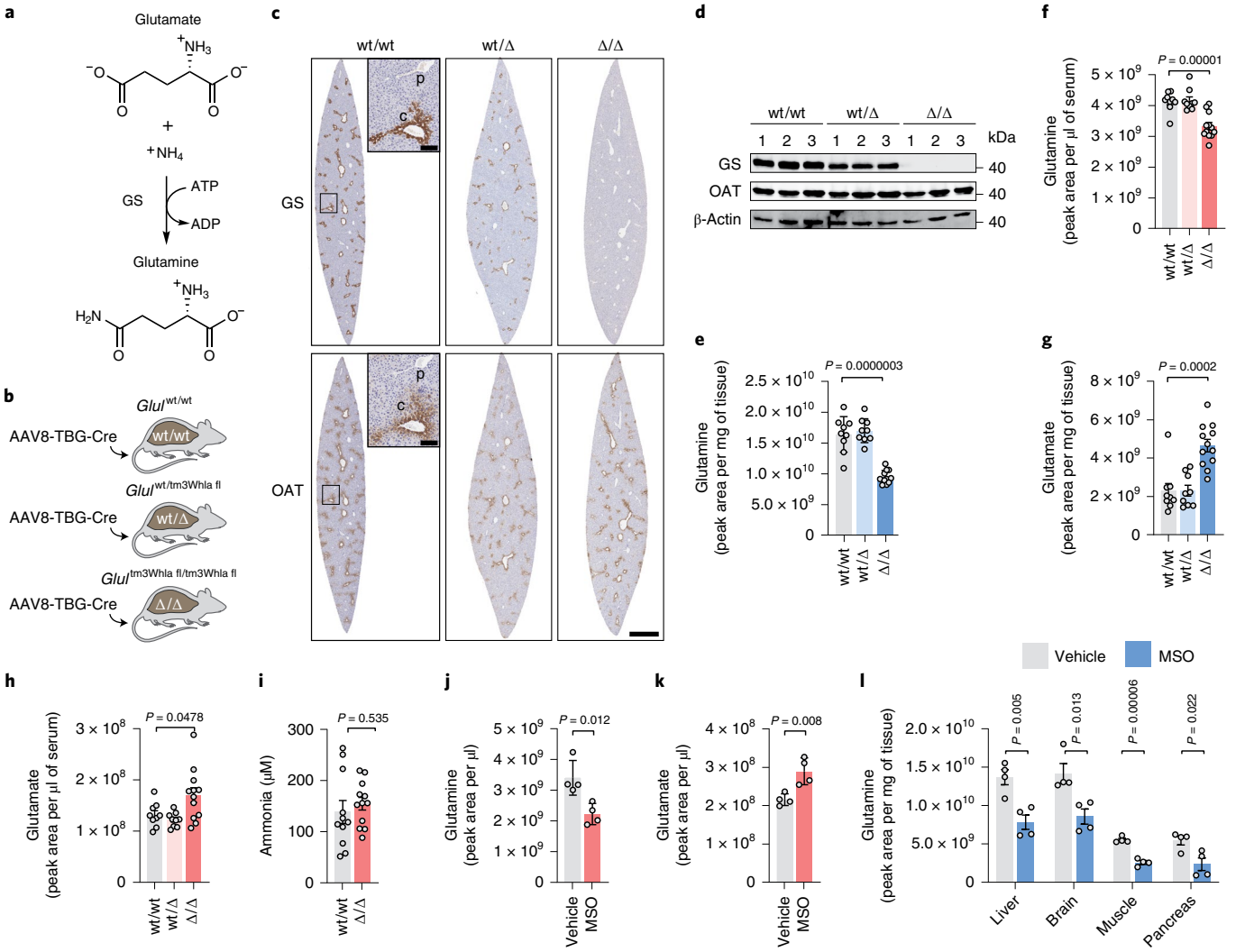

Fig. 1 | Effects of liver GS deficiency on glutamine metabolism. a, GS-catalyzed reaction. **b**, Administration of AAV8-TBG-Cre in mice with wt/wt, *Glul*$^{wt/tm3Whla\ fl}$ and *Glul*$^{tm3Whla\ fl/tm3Whla\ fl}$ genotypes results in mice with wt/wt, wt/Δ and Δ/Δ livers, respectively. **c**, Serial sections of mouse liver stained by IHC for GS and OAT, two markers of pericentral zones; scale bar, 1 mm. The insets show magnifications of the central vein (c) and portal vein (p); scale bar, 100 µm. The images shown are representative of three mice per genotype. **d**, Immunoblot of liver samples obtained from $n = 3$ mice per genotype. β-Actin is shown as a loading control. **e**,**f**, Glutamine levels in wt/wt ($n = 9$), wt/Δ ($n = 9$) and Δ/Δ ($n = 12$) livers (**e**) and sera (**f**) measured by LC–MS. **g**,**h**, Glutamate levels in the livers (**g**) and sera (**h**) of wt/wt ($n = 9$), wt/Δ ($n = 9$) and Δ/Δ ($n = 12$) mice. **i**, Ammonia concentration in blood samples from wt/wt ($n = 11$) and Δ/Δ ($n = 12$) mice. **j**,**k**, Glutamine (**j**) and glutamate (**k**) levels in the blood collected from mice 4 h after administration of vehicle ($n = 4$) and MSO ($n = 4$). **l**, Glutamine levels in the liver, brain, muscle and pancreas from mice treated as in **j** ($n = 4$ vehicle, $n = 4$ MSO). Data in **e**–**l** were analyzed by two-tailed Student's *t*-test. Bars represent mean ± s.e.m., and each circle represents data from a single mouse.

in blood circulation. While the mechanism of ammonia toxicity of the central nervous system is not fully understood, the clinical manifestations of severe hyperammonemia include impaired brain functions, known as hepatic encephalopathy, that can lead to brain injury and death[8]. Hepatic GS is selectively expressed in hepatocytes surrounding the central veins, where residual ammonia that has not been detoxified by the urea cycle is incorporated into the amidic group of glutamine by an ATP-dependent reaction that uses glutamate as cosubstrate[8,9] (Fig. 1a). Hence, the role of GS in physiopathology has been studied both in relation to its ammonia-clearing and glutamine-producing activities[4,8–11].

We applied orthogonal pharmacological and genetic approaches in mouse and cellular models to show that the metabolic effects of GS extend beyond the regulation of its canonical substrates and product and connect microbiome and hepatic metabolism by synthesizing N^5-methylglutamine.

Results

Metabolic effects of hepatic GS deletion

The deletion of *Glul* in the hepatocytes of adult mice carrying the *Glul*^{tm3Whla} floxed allele (*Glul*$^{tm3Whla\ fl}$)[8] was achieved by administering adeno-associated virus with TBG promoter-driven expression of Cre (AAV8-TBG-Cre; Fig. 1b)[12,13]. While heterozygous deletion of hepatic *Glul* (wild type/Δ (wt/Δ)) caused an ~40% decrease in GS expression (Fig. 1c,d), homozygous deletion (Δ/Δ) resulted in complete liver-specific loss of GS (Fig. 1c,d and Extended Data Fig. 1a), without affecting the expression of ornithine aminotransferase (OAT), another metabolic marker of the pericentral zone (Fig. 1c,d). Hereafter, mice with liver-specific recombined *Glul*$^{tm3Whla\ fl}$ alleles are referred to as wt/wt, wt/Δ and Δ/Δ. GS deletion did not affect body or liver weight (Extended Data Fig. 1b,c), and, in accordance with human GS deficiency syndrome, the heterozygous deletion of GS did not result in appreciable metabolic changes (Fig. 1e–h)[14]. Despite GS expression being limited to

https://doi.org/10.1038/s41589-022-01154-9

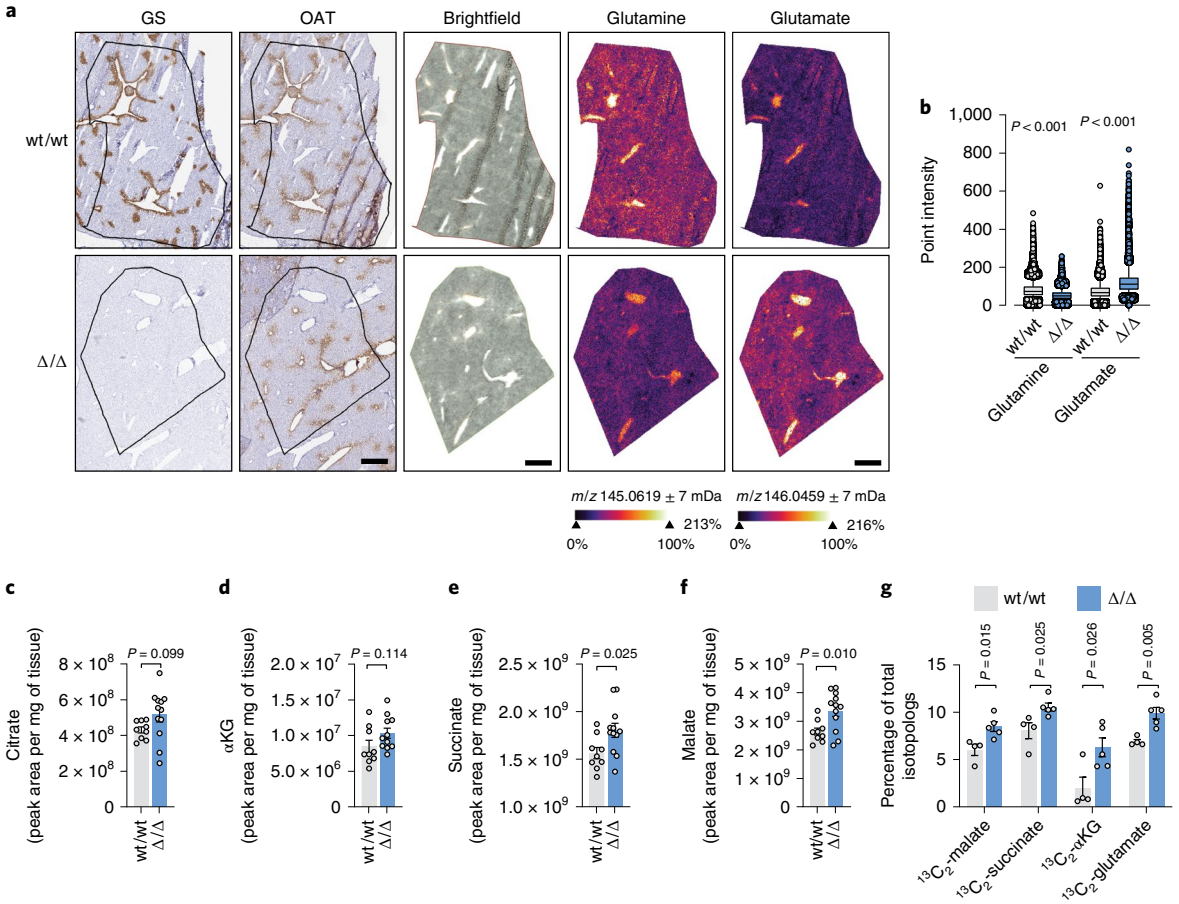

Fig. 2 | Metabolic imaging and glucose tracing in GS-deficient liver. **a**, Serial sections of frozen liver samples from wt/wt and Δ/Δ female mice. Left, IHC staining for GS and OAT. Right, MS metabolic imaging of glutamine and glutamate. Data were normalized with the root mean square method; scale bar, 1 mm. Images are representative of $n = 3$ livers per genotype (Extended Data Fig. 1d,e). **b**, Quantification of glutamine and glutamate in the regions of interest shown in **a** ($n = 1$ wt/wt, $n = 1$ Δ/Δ). Boxes have bounds at the 25th to 75th percentiles, the lines represent the medians and whiskers show the 5th to 95th percentiles; each data point represents the relative intensity of one pixel. Data were analzyed by two-tailed Student's *t*-test. **c**–**f**, Levels of citrate (**c**), α-ketoglutarate (αKG; **d**), succinate (**e**) and malate (**f**) in the livers of wt/wt ($n = 9$) and Δ/Δ ($n = 12$) mice. **g**, Relative levels of $^{13}C_2$ isotopolog in the livers of wt/wt ($n = 4$) and Δ/Δ ($n = 5$) mice administered U-$^{13}C_6$-glucose. Data were analyzed by two-tailed Student's *t*-test. Bars represent mean ± s.e.m., and each circle represents data from a single mouse.

only ~7% of all hepatocytes, its homozygous deletion caused an ~40% decrease in glutamine levels in the liver (Fig. 1e) and an ~20% decrease in systemic blood circulation (Fig. 1f). Whereas circulating ammonia levels were not significantly altered (Fig. 1i), glutamate levels were elevated in Δ/Δ liver and serum (Fig. 1g,h). Comparable results for the circulating levels of glutamine and glutamate were obtained after treatment with methionine sulfoximine (MSO; Fig. 1j,k), an irreversible GS inhibitor that decreased glutamine levels in GS-expressing organs, including the liver, brain, muscle and pancreas (Fig. 1l).

To determine if the distinctive zonation of GS expression in the liver could affect the levels of glutamine and glutamate in different metabolic zones, we applied mass spectrometry (MS)-based metabolic imaging. In wt/wt liver, glutamine and glutamate levels were comparable between pericentral (GS^+OAT^+) and periportal (GS^-OAT^-) areas (Fig. 2a). Consistently, GS deletion decreased glutamine levels and increased glutamate levels throughout the liver tissue (Fig. 2a,b and Extended Data Fig. 1d,e), suggesting that GS activity determines glutamine and glutamate concentrations across the different metabolic zones of the liver lobule.

The ~30% increase in circulating levels of glutamate observed in Δ/Δ mice (Fig. 1h) demonstrates that hepatic glutamine synthesis regulates systemic glutamate metabolism[15]. However, the increased hepatic levels of tricarboxylic acid (TCA) cycle intermediates observed in Δ/Δ liver (Fig. 2c–f) are suggestive of a decreased flux draining from the TCA to glutamine (that is, cataplerotic) imposed by the lack of glutamine synthesis. To directly investigate this hypothesis, we traced $^{13}C_6$-glucose in wt/wt and Δ/Δ mice. The results showed that the enrichment in glucose-derived carbons of malate, succinate, α-ketoglutarate and glutamate is higher in Δ/Δ than in wt/wt livers (Fig. 2g and Extended Data Fig. 1f). Together, these results demonstrate that the hepatic synthesis of glutamine is fueled at least in part by in situ glutamate production from glucose.

In vivo levels of N^5-methylglutamine are GS dependent

To broaden our understanding of the role of GS in liver metabolism, we performed a liquid chromatography–MS (LC–MS)-based untargeted analysis on Δ/Δ livers and on livers from mice treated with MSO. The comparisons with the respective controls revealed an unexpected feature with a predicted molecular weight of 160.08479 ± 1.2 ppm and a molecular formula of $C_6H_{12}N_2O_3$ that was significantly downregulated after GS deletion or pharmacological inhibition (Fig. 3a,b). The corresponding extracted ion chromatograms revealed a peak with lower intensity in Δ/Δ and MSO-treated livers than in respective controls (Fig. 3c). Quantification of the normalized peak areas showed decreases of ~75% and ~80% in Δ/Δ and MSO-treated livers, respectively, compared to controls (Fig. 3d,e). $C_6H_{12}N_2O_3$ levels were also decreased in the sera

https://doi.org/10.1038/s41589-022-01154-9

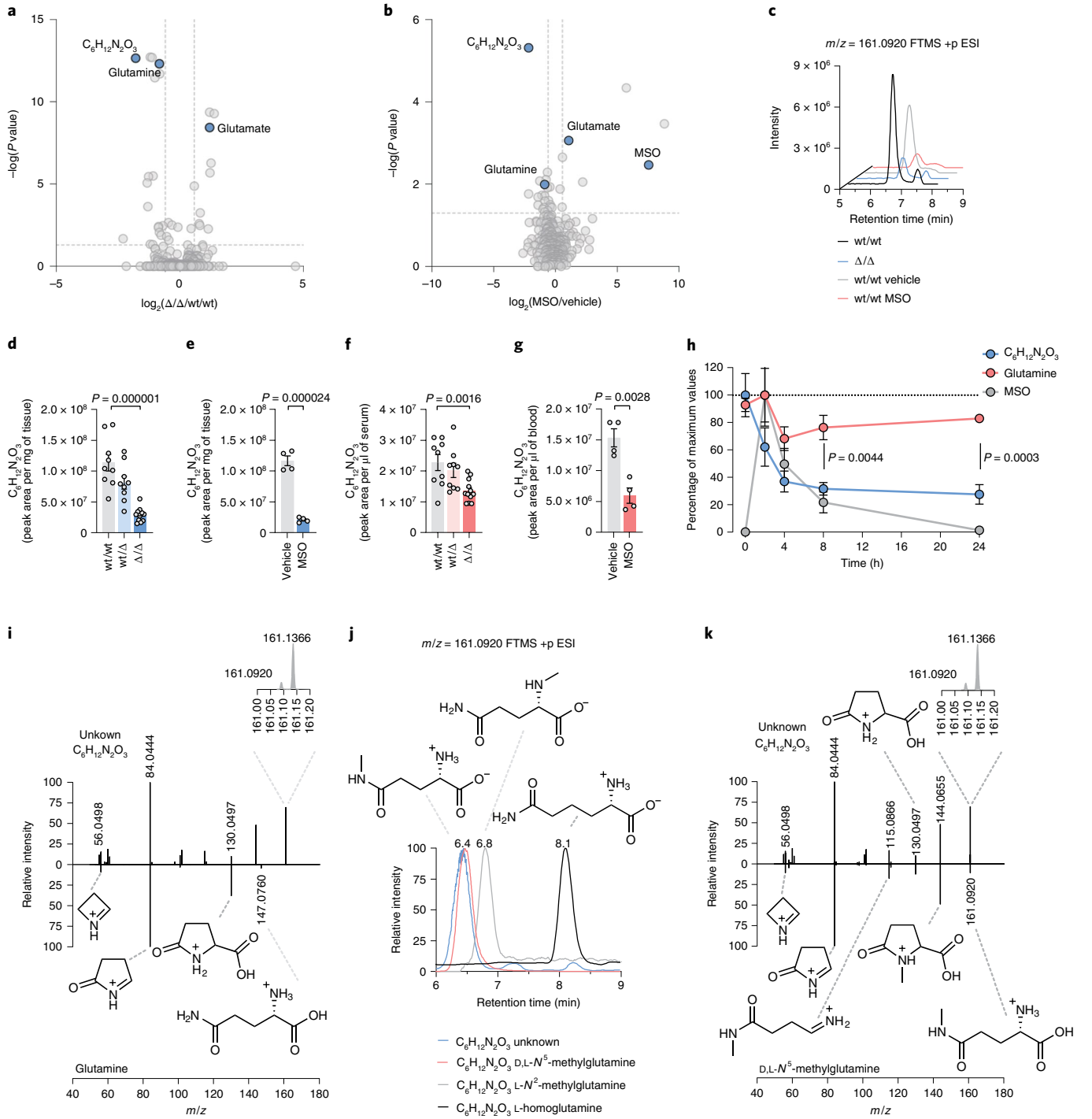

Fig. 3 | Untargeted metabolomics reveals N^5-methylglutamine as a GS product. a,**b**, Manually curated volcano plots obtained from an untargeted metabolomic analysis of livers from wt/wt ($n = 9$) and Δ/Δ ($n = 12$) mice (**a**) or from mice treated with vehicle ($n = 4$) or MSO ($n = 4$) (**b**). Data were analyzed by analysis of variance and Tukey honest significant difference post hoc test. **c**, Extracted ion chromatograms of one representative liver sample from mice described in **a** and **b**. FTMS +p ESI, Fourier transform mass spectometry in positive polarity coupled with electrospray ionisation. **d**,**e**, Levels of the compound with formula $C_6H_{12}N_2O_3$ in the livers of wt/wt ($n = 9$), wt/Δ ($n = 9$) and Δ/Δ ($n = 12$) mice (**d**) or in the livers collected from mice 4 h after administration of vehicle ($n = 4$) or MSO ($n = 4$) (**e**). **f**,**g**, Levels of the compound with formula $C_6H_{12}N_2O_3$ in the sera (**f**) or blood (**g**) of mice described in **d** and **e**. Data in **d**–**g** were analyzed by two-tailed Student's *t*-test. **h**, Relative levels of the compound with formula $C_6H_{12}N_2O_3$ in the blood of vehicle-treated ($n = 4$) or MSO-treated ($n = 4$) mice. MSO was administered immediately after the first blood collection at 0 h. For each metabolite, the percentage of the maximal peak area values averaged at each time point is reported. Data were analyzed by two-tailed Student's *t*-test. Circles represent mean ± s.e.m. ($n = 4$). **i**, Mirror plot of MS/MS spectra from wt/wt liver samples ($n = 2$) comparing parent and fragment ions generated from the compound with formula $C_6H_{12}N_2O_3$ (top) to glutamine (bottom). The inset shows a magnified *m/z* range of 161.0 to 161.2 showing the ion of interest (*m/z* 161.0920) and a coisolated ion (*m/z* 161.1366). The structures of putative glutamine fragments are shown (Extended Data Fig. 2b). **j**, Overlaid extracted ion chromatograms of *m/z* 161.0920 obtained from a wt/wt liver sample ($n = 1$, $C_6H_{12}N_2O_3$ unknown), D,L-N^5-methylglutamine standard, L-N^2-methylglutamine standard and L-homoglutamine standard. The retention times and molecular structures of these compounds are shown. **k**, Mirror plot of MS/MS data from a wt/wt liver sample ($n = 1$) comparing the compound with formula $C_6H_{12}N_2O_3$ (top) to D,L-N^5-methylglutamine standard (bottom). The proposed structures of parent and fragment ions derived from D,L-N^5-methylglutamine are shown (Extended Data Fig. 2c).

of Δ/Δ and MSO-treated mice (~60% and ~50%, respectively; Fig. 3f,g). Circulating levels of $C_6H_{12}N_2O_3$, glutamine and MSO were monitored for 24 h after administration of MSO (Fig. 3h). MSO levels reached a maximum of 18.6 ± 7.2 µM (mean ± s.d.; $n = 4$) 2 h after administration and decreased to 0 at 24 h. Glutamine levels transiently dropped between 2 and 4 h but recovered thereafter. Conversely, the levels of $C_6H_{12}N_2O_3$ progressively diminished after MSO administration, reaching ~27% of the initial levels at 24 h. These results demonstrate that the circulating levels of glutamine and $C_6H_{12}N_2O_3$ respond to irreversible GS inhibition with different kinetics, suggesting that alternative sources of glutamine (for example, diet or autophagy) may compensate for the lack of glutamine synthesis, while $C_6H_{12}N_2O_3$ production strictly depends on GS activity.

To identify the compound with formula $C_6H_{12}N_2O_3$, we analyzed wt/wt livers using tandem mass spectrometry (MS/MS). The comparison of the fragmentation patterns of glutamine ($C_5H_{10}N_2O_3$) and $C_6H_{12}N_2O_3$ revealed the presence of three common fragments (m/z 56.0498, 84.0444 and 130.0497; Fig. 3i), supporting the hypothesis of $C_6H_{12}N_2O_3$ being a glutamine analog with an additional methylene or methyl group. The addition of a methylene group to the glutamine carbon backbone could lead to L-homoglutamine, reported on one occasion to be synthesized by mammalian GS from α-aminoadipic acid and ammonia (Extended Data Fig. 2a)[16]. However, the analytical standard for L-homoglutamine was chromatographically separated from the unknown compound present in liver extracts, refuting this hypothesis (Fig. 3j). Next, we tested the chromatographic response of two glutamine analogs with the methyl group bound to either the aminic (N^2-methylglutamine) or amidic nitrogen (N^5-methylglutamine). The two compounds were chromatographically separated, and the retention time of N^5-methylglutamine coincided with that of the unknown compound present in the liver samples (Fig. 3j). Further MS/MS analysis showed matching fragmentation patterns for the analytical standard and the unknown compound (common fragments m/z 56.0498, 84.0444, 115.0866, 130.0497 and 144.0655), identifying it as N^5-methylglutamine (Fig. 3k; proposed mechanisms of fragmentation for glutamine[17] and N^5-methylglutamine are shown in Extended Data Fig. 2b,c).

Human GS synthesizes N^5-methylglutamine in vitro

To our knowledge, the biosynthesis of N^5-methylglutamine has not been reported in mammals, and in bacteria, N^5-methylglutamine can be obtained by the transfer of a methyl group from a methyl donor, such as *S*-adenosyl-L-methionine, as described for peptide-bound glutamine[18], or by the nucleophilic attack of methylamine to the γ-carboxylic group of glutamate (Fig. 4a)[19,20].

To demonstrate that GS is the source of N^5-methylglutamine and test if methylamine is used as substrate, we used purified human recombinant GS. The LC–MS analysis of the reaction mixture containing methylamine sampled at the reaction start and after 60 min demonstrated that GS production of N^5-methylglutamine is ATP dependent (Fig. 4b and Extended Data Fig. 3a). Moreover, if equimolar amounts of ammonia and methylamine were added to the recombinant GS, N^5-methylglutamine and glutamine were synthesized with a stoichiometric ratio of 1:65 (Extended Data Fig. 3b).

Next, we tested if human cells could produce N^5-methylglutamine. GS expression is high in liver and brain, and we found that cancer cell lines derived from these organs (HepG2 and T16 (ref. [21])) produce N^5-methylglutamine after supplementation of methylamine (Fig. 4c,d), whereas Cas9-mediated deletion of GS in HepG2 cells significantly inhibited N^5-methylglutamine production (Fig. 4c). Comparable results were obtained by inhibiting GS with MSO treatment in both HepG2 and T16 cell lines (Fig. 4c,d). To assess the relevance of the newly described activity of GS to human pathology, we investigated pathogenic mutations affecting the GS active site (Fig. 4e), which cause a rare inborn error of metabolism called GS deficiency[14]. First, we purified a human recombinant GS with the R324C mutation (Extended Data Fig. 3c–f) and found that this mutation decreased the affinity for ammonia (Fig. 4f) more than that for methylamine (Fig. 4g). Subsequently, we tested the effects of pathogenic mutations in HEK293 cells where the endogenous *GLUL* alleles were deleted (GS KO), and wt GS or the R324C and R324A mutants were reexpressed. In cells expressing R324C and R324A mutants, glutamine levels were reduced by half compared to cells expressing wt GS (Fig. 4h), in line with the decreased glutamine levels found in individuals with GS mutations[14]. Conversely, cellular levels of N^5-methylglutamine were markedly increased by the mutant variants compared to the wt control (Fig. 4i). These observations indicate that these mutations disproportionately affect the catalytic activity of GS with high affinity for ammonia (approximately fourfold; Fig. 4f), conferring a competitive advantage to the low-affinity substrate methylamine (Fig. 4g). Altogether, these results demonstrate that human GS synthesizes N^5-methylglutamine from glutamate and methylamine and show that this alternative activity is favored by human pathogenic mutations occurring at the active site of the enzyme.

Methylamine is a GS substrate in vivo

To test if N^5-methylglutamine could also be produced by methylation of glutamine, we traced $^{13}C_5$-glutamine in wt/wt mice. Although $^{13}C_5$-glutamine levels in circulation were significantly increased, $^{13}C_5$-N^5-methylglutamine remained undetectable (Extended Data Fig. 4a,b), strengthening the in vivo validity of the working model where N^5-methylglutamine is synthesized by GS from glutamate and methylamine. To investigate whether systemic methylamine could modulate the production of N^5-methylglutamine, we injected ^{13}C-methylamine into wt/wt and Δ/Δ mice. The administration of ^{13}C-methylamine did not significantly perturb circulating glutamine levels (Extended Data Fig. 4c). By contrast, ^{13}C-N^5-methylglutamine levels peaked at 2 h after ^{13}C-methylamine injection, at which point the levels reached in Δ/Δ mice were significantly lower than those in wt/wt mice (Fig. 5a). Consistently, the levels of ^{13}C-N^5-methylglutamine in the liver were approximately tenfold lower in Δ/Δ mice than in wt/wt mice (Fig. 5b). This demonstrates that N^5-methylglutamine levels are modulated in vivo by circulating methylamine via hepatic GS activity. Similarly, N^5-methylglutamine levels were markedly decreased (approximately fivefold) in the Δ/Δ liver compared to wt/wt in mice supplemented for 5 months with 0.1% (wt/vol) methylamine in the drinking water (Extended Data Fig. 4d). Next, we performed untargeted metabolomics on liver tissue samples from wt/wt and Δ/Δ mice untreated or chronically supplemented with methylamine. To identify the metabolic effects specific for the liver-produced N^5-methylglutamine, we ranked the metabolic features based on their Pearson correlation coefficients with N^5-methylglutamine levels (Extended Data Fig. 4e). The ranking identified α-ketoglutarate as the metabolic feature with the second most stringent anticorrelation with N^5-methylglutamine (Pearson $r = -0.67$ and $P = 0.003$; Extended Data Fig. 4e,f). In fact, α-ketoglutarate levels were significantly decreased by methylamine in wt/wt but not in Δ/Δ livers (Extended Data Fig. 4g), suggesting that N^5-methylglutamine could negatively regulate hepatic levels of α-ketoglutarate.

N^5-Methylglutamine synthesis is sustained by the microbiome

It has been shown that methylamine can be produced by the human enzyme PAD4 during the demethylimination of histone methyl-arginine[22]. Moreover, the levels of methylamine excreted in urine increase after sarcosine administration in rats[23] and choline ingestion in humans[24]. However, the metabolic origin of methylamine in liver tissue (~41 µM; Extended Data Fig. 4h) is not fully understood. In analogy to the production of trimethylamine, which largely depends on intestinal microbiome metabolism[25], we tested whether methylamine production could also be microbiota dependent. In line with this hypothesis, the concentration of methylamine in serum sampled from the portal vein was twofold higher (16 µM) than the concentration found

https://doi.org/10.1038/s41589-022-01154-9

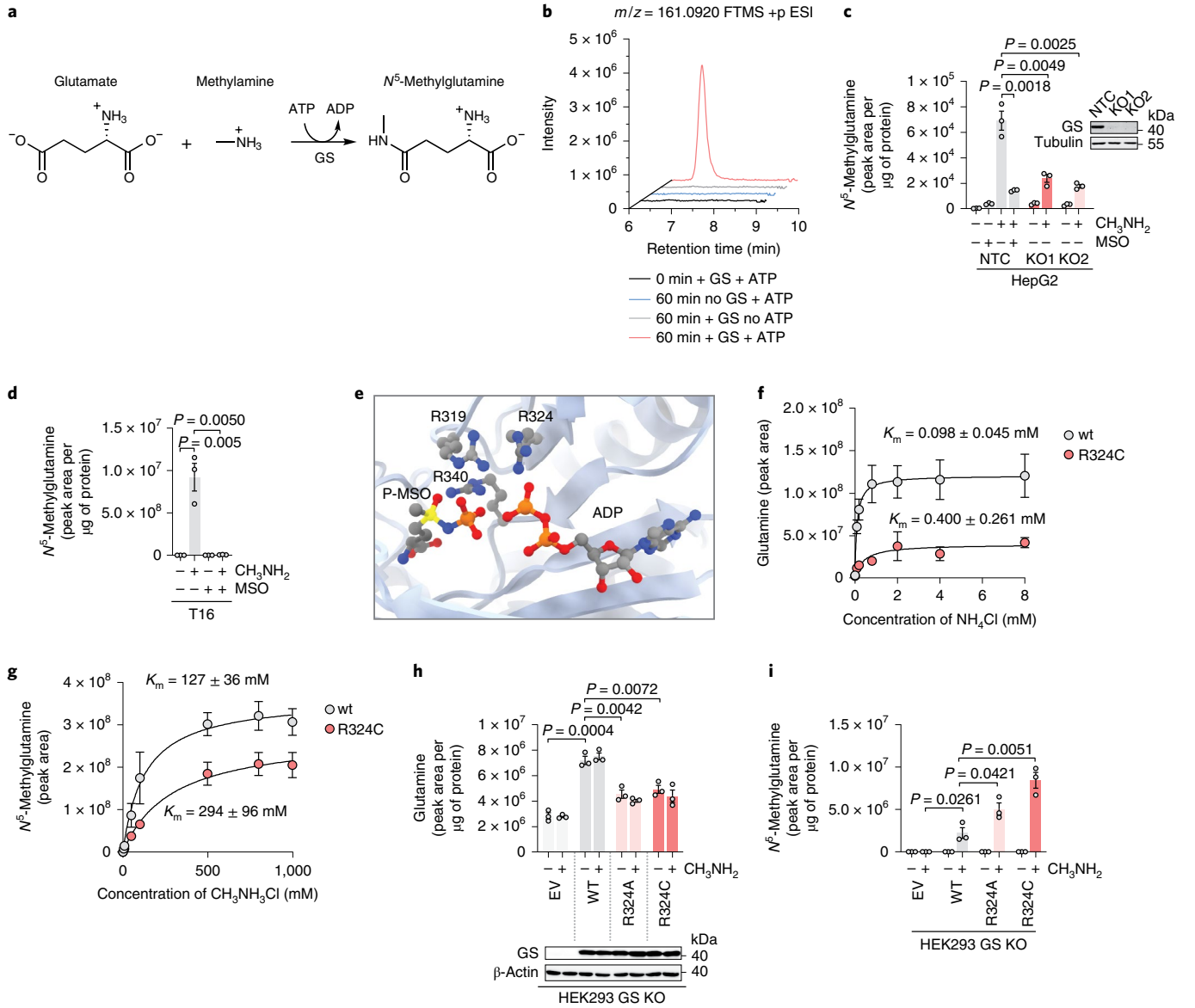

Fig. 4 | GS synthesizes N^5-methylglutamine from glutamate and methylamine. a, Non-canonical reaction catalyzed by GS. **b**, Reaction mixtures described in the Methods and modified as indicated in the figure were sampled at 0 and 60 min from the addition of 40 mM methylamine. Representative extracted ion chromatograms for *m/z* 161.0920 are shown. **c**, HepG2 cells deficient for GS (KO1 and KO2) or non-targeting control (NTC) were grown in glutamine-free medium for 24 h and incubated with methylamine (CH_3NH_2, 0.8 mM) or MSO (1 mM) for an additional 24 h. Data were analyzed by two-tailed Student's *t*-test. Bars represent mean ± s.e.m., and each data point represents an independent experiment ($n = 3$). The inset shows immunoblotting analysis of GS. Tubulin is shown as a loading control ($n = 1$). **d**, T16 cells were incubated with methylamine (0.4 mM) or MSO (1 mM) as indicated for 48 h. Data were analyzed by two-tailed Student's *t*-test. Bars represent mean ± s.e.m., and each data point represents an independent experiment ($n = 3$). **e**, The active site of human GS with highlighted arginine residues, phospho-MSO (P-MSO) and ADP (PDB 2QC8 visualized with UCSF Chimera v1.15). **f**,**g**, GS wt and mutant proteins were purified as described in the Methods and in Extended Data Fig. 3c–f. K_m values for ammonia (**f**) and methylamine (**g**) were calculated using the Michaelis–Menten equation. Samples were collected from the reaction mixtures 15 min after methylamine or ammonia addition. Data points represent mean ± s.e.m. of $n = 3$ independent experiments. **h**,**i**, HEK293 cells deleted for GS (GS KO) were transfected with an empty vector (EV) control or vectors encoding GS wt or R324A and R324C mutant variants. Twenty-four hours after transfection, cells were incubated with methylamine (0.4 mM) for an additional 24 h, and glutamine (**h**), GS (**h** immunoblot inset; β-actin is shown as a loading control; $n = 1$) and N^5-methylglutamine (**i**) levels were measured. Data were analyzed by two-tailed Student's *t*-test. Bars represent mean ± s.e.m., and each data point represents an independent experiment ($n = 3$).

in the systemic circulation (Extended Data Fig. 4i). To further investigate the role of the microbiome, age-matched germ-free mice were orally administered either sterile PBS or a solution containing the microbiota derived from a specific pathogen-free (SPF) donor. The sera obtained from microbiome-reconstituted mice showed that methylamine levels were significantly increased compared to germ-free mice (Fig. 5c). Consequently, the levels of N^5-methylglutamine increased by ~50% in sera and by ~30% in liver tissue of mice with an active microbiome (Fig. 5d,e). These results demonstrate that hepatic GS mediates the conversion of microbiome-derived methylamine to N^5-methylglutamine.

Liver β-catenin mutation drives N^5-methylglutamine synthesis

It has been shown that *GLUL* is a direct transcriptional target of β-catenin in the liver[26]. The activation of the WNT/β-catenin signaling pathway drives human liver carcinogenesis, thus representing a pathological condition where GS overexpression has clinical significance[27].

https://doi.org/10.1038/s41589-022-01154-9

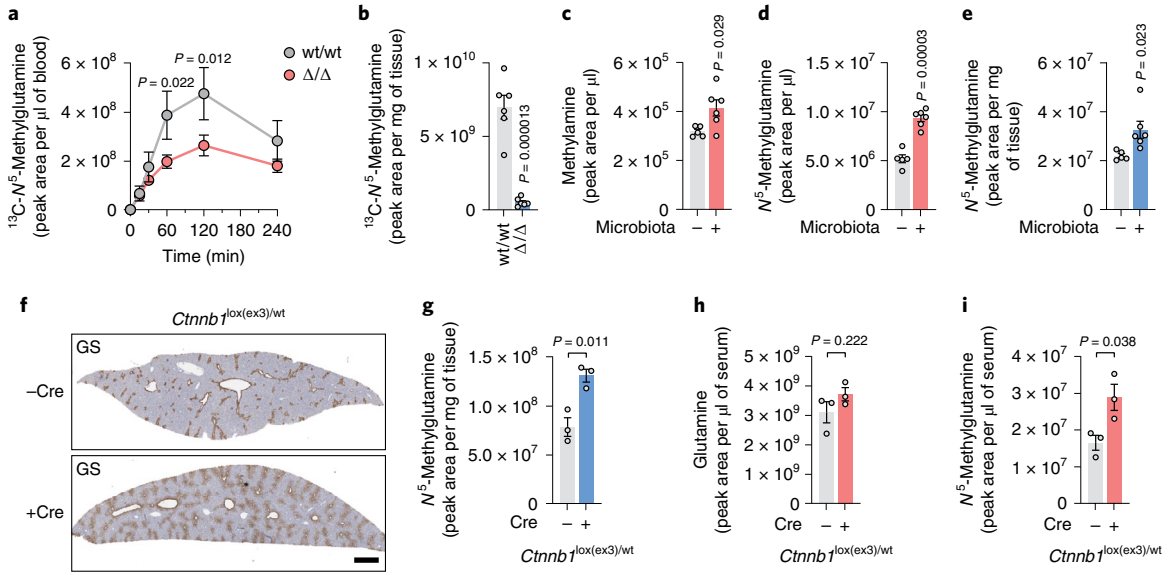

Fig. 5 | The microbiome and β-catenin activation increase N^5-methylglutamine synthesis. a, ^{13}C-N^5-Methylglutamine levels in the blood of wt/wt ($n = 3$) and Δ/Δ ($n = 3$) mice immediately before and 15, 30, 60, 120 and 240 min after injection of ^{13}C-methylamine (2 mmol per kg body weight). *P* values refer to the comparison of wt/wt to Δ/Δ levels at 60 and 120 min. **b**, ^{13}C-N^5-Methylglutamine levels in the livers of wt/wt ($n = 6$) and Δ/Δ ($n = 6$) mice 2 h after ^{13}C-methylamine administration. **c**–**e**, Methylamine (**c**) and N^5-methylglutamine (**d**) levels in the sera and N^5-methylglutamine levels in the liver tissue (**e**) of female germ-free mice administered with vehicle control ($n = 5$) or with SPF microbiota ($n = 6$). **f**, Representative images of IHC staining for GS in livers of *Cnntb1*$^{fl(ex3)/wt}$ male mice 4 d after administration of AAV8-Null-Cre or AAV8-TBG-Cre; scale bar, 1 mm. **g**, Levels of N^5-methylglutamine in the livers of AAV8-Null-Cre ($n = 3$) or AAV8-TBG-Cre ($n = 3$) mice described in **f**. **h**,**i**, Glutamine (**h**) and N^5-methylglutamine (**i**) levels in the sera of the mice ($n = 3$) described in **f**. Data in **a**–**e** and **g**–**i** were analyzed by two-tailed Student's *t*-test. Bars represent mean ± s.e.m.

To test if oncogenic β-catenin activation could modulate the non-canonical activity of GS, we administered AAV8-TBG-Cre to adult mice carrying one copy of the *Ctnnb1*$^{lox(ex3)}$ allele[28]. The deletion of exon 3 from *Ctnnb1* resulted in the expression of a constitutively active β-catenin in the liver, causing expansion of the GS$^+$ zone (Fig. 5f) and consequent accumulation of N^5-methylglutamine in liver tissue (Fig. 5g). Remarkably, while glutamine levels were not significantly altered in the sera of β-catenin-mutant mice (Fig. 5h), N^5-methylglutamine was increased by ~75% compared to Cre$^-$ controls (Fig. 5i). These results confirmed that circulating N^5-methylglutamine is a stringent readout for hepatic GS expression, suggesting its possible use as a biomarker for β-catenin-mutant hepatocellular carcinoma (HCC).

N^5-Methylglutamine as a biomarker for GS-expressing HCC

To further test the validity of this hypothesis, we generated a mouse model of liver cancer driven by the combined expression of *Ctnnb1*$^{lox(ex3)}$ and MYC (*Rosa26*$^{DM.lsl\text{-}MYC/DM.lsl\text{-}MYC}$)[29], two oncogenic events co-occurring in HCC.

The administration of AAV8-TBG-Cre resulted in liver-specific neoplastic lesions that progressed to clinical endpoint with a median survival of 131 and 161 d after induction for male and female mice, respectively. Crucially, we observed tumor-specific high expression of GS (Extended Data Fig. 4j). The ratio between liver volume, measured in live mice by magnetic resonance imaging (MRI), and body weight was used as an index for tumor burden (Fig. 6a). Urine samples were collected before MRI from seven tumor-bearing mice and one age-matched wt/wt control mouse. N^5-Methylglutamine was detectable in the urine of wt/wt mice, and its creatinine-normalized levels were increased in all mice with β-catenin/c-MYC-driven tumors, demonstrating a significant positive correlation with tumor burden (Pearson $r = 0.8$ and $P = 0.016$; Fig. 6b). Further, the normalized urine levels of N^5-methylglutamine and glutamine were measured during tumor progression along with liver volumes. The results show that N^5-methylglutamine, but not glutamine, increases synchronously with the tumor burden (Fig. 6c). To ascertain the causal link between GS expression in the tumors and N^5-methylglutamine levels, we generated a line of mice with the *Ctnnb1*$^{lox(ex3)}$, MYC (*Rosa26*$^{DM.lsl\text{-}MYC/DM.lsl\text{-}MYC}$) and *Glul*$^{tm3Whla\ fl}$ alleles. The administration of AAV8-TBG-Cre to these mice did not affect the expression of GS in the untransformed liver and resulted in β-catenin/c-MYC-driven tumors deleted for GS (Fig. 6d). The urine and circulating levels of N^5-methylglutamine from these mice were significantly lower than those from mice with GS-expressing tumors (Fig. 6e and Extended Data Fig. 4k). Finally, we found that N^5-methylglutamine urine levels were not increased in mice with GS$^-$ p53-null/c-MYC liver tumors or in mice with GS$^+$ pancreatic tumors (*Kras*$^{LSL.G12D/+}$; *Trp53*$^{R172H/+}$; *Pdx1*-Cre (KPC))[11] compared to tumor-free mice (Fig. 6e and Extended Data Fig. 4l), strengthening the validity of this newly discovered GS-derived metabolite as a selective biomarker for β-catenin-mutant liver cancer.

Discussion

In this study, we demonstrated that GS accepts methylamine as a substrate for the ATP-dependent synthesis of N^5-methylglutamine. The gene encoding GS is one of the most ancient genes found in all forms of life[1]. Hence, it is reasonable to speculate that alongside glutamine synthesis, this previously unreported activity of GS was selected during evolution. The identification of N^5-methylglutamine opens new avenues of research to investigate the relevance of its biosynthesis in the physiopathology of organs with high expression of GS. N^5-Methylglutamine is a glutamine analog, and its biological functions could interfere with glutamine transport and catabolism. Indeed, our results suggest that N^5-methylglutamine regulates the hepatic levels of α-ketoglutarate, a product of glutamine degradation with important metabolic and signaling functions[30]. Despite the apparent low affinity of GS toward methylamine observed in vitro with recombinant enzymes and cells, GS activity in the pericentral hepatocytes controls the urine, serum and hepatic concentrations of N^5-methylglutamine, ~10 µM, ~0.8 µM and ~24 µM, respectively (Extended Data Fig. 4m–o).

The non-canonical activity of GS in the liver is fed by the methylamine produced by the microbiota, as demonstrated by inoculating

https://doi.org/10.1038/s41589-022-01154-9

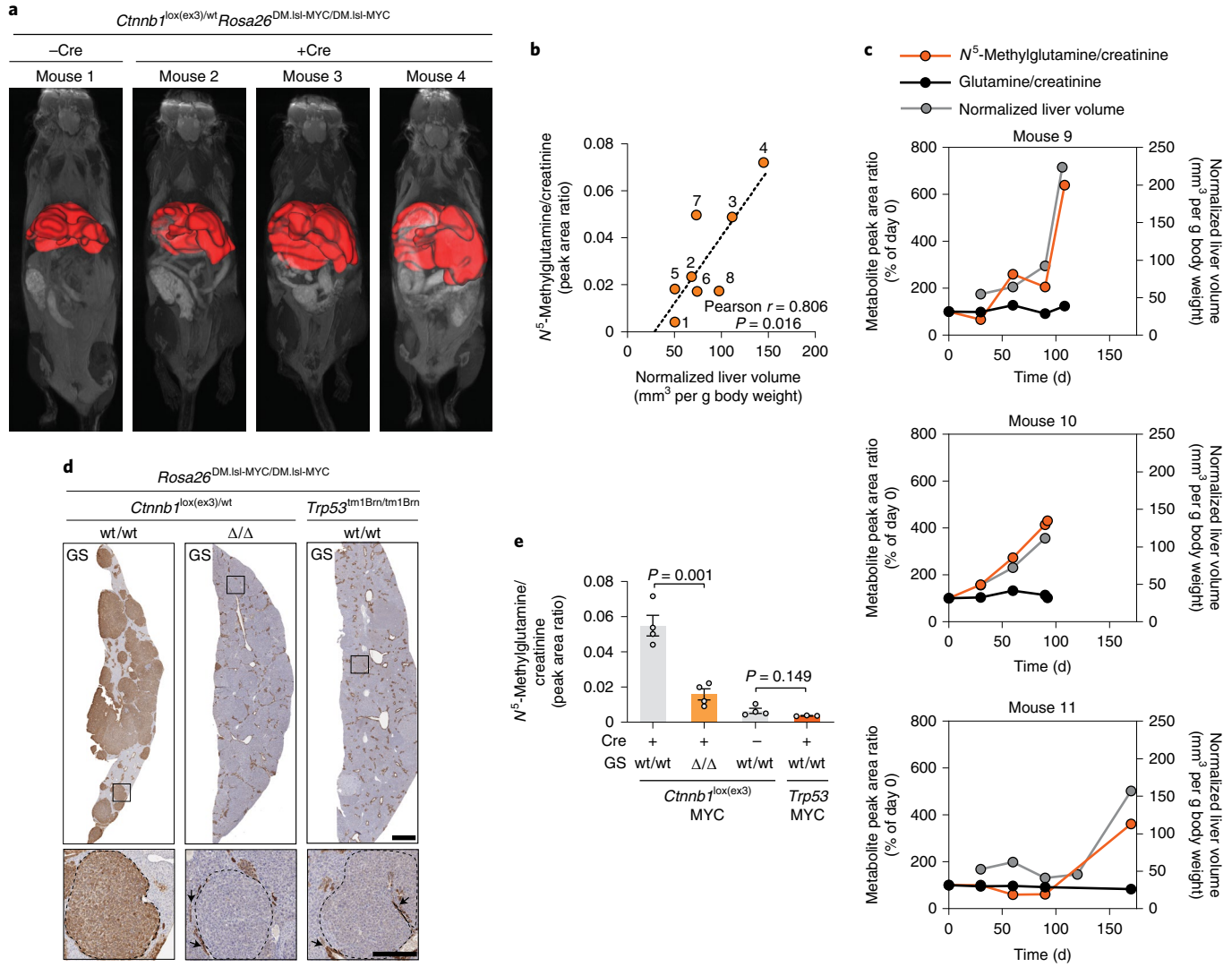

Fig. 6 | N^5-Methylglutamine levels correlate with GS$^+$ liver tumor progression. **a**, MRI images of *Cnntb1*$^{fl(ex3)/wt}$*Rosa26*$^{DM.lsl\text{-}MYC/DM.lsl\text{-}MYC}$ mice scanned 121–156 d after administration of AAV8-TBG-Cre (mice 2, 3 and 4, females). A non-induced mouse (1, female) is shown as a control. Three-dimensional reconstructions of the livers are highlighted in red. **b**, Correlation between the normalized levels of N^5-methylglutamine in the urine of eight mice (1–7, females; 8, male) described in **a** and their normalized liver volumes. Urine samples were collected 24–48 h before the MRI. Data were analyzed by two-tailed Pearson correlation analysis ($n = 8$). **c**, Normalized urine levels of N^5-methylglutamine and glutamine and normalized liver volumes measured in three male mice with the genotype described in **a**. Day 0 corresponds to the day of AAV8-TBG-Cre administration. Individual data points are shown for three mice. **d**, Representative images of IHC staining for GS in liver sections from *Ctnnb1*$^{lox(ex3)/wt}$*Rosa26*$^{DM.lsl\text{-}MYC/DM.lsl\text{-}MYC}$ male mice with wt/wt or Δ/Δ alleles and *Rosa26*$^{DM.lsl\text{-}MYC/DM.lsl\text{-}MYC}$*Trp53*$^{tm1brn/tm1brn}$ male mice. Mice were sampled at clinical endpoints between 55 and 164 d after AAV8-TBG-CRE administration; scale bar, 1 mm. The insets show magnifications of tumor regions delineated by dotted lines; scale bar, 250 µm. Arrows indicate normal GS$^+$ hepatocytes surrounding central veins. **e**, Normalized urine levels of N^5-methylglutamine from the mice described in **d** ($n = 4$, *Ctnnb1* MYC; $n = 3$, *Trp53* MYC) or in age-matched control male mice administered AAV8-Null-Cre ($n = 4$). Data were analyzed by two-tailed Student's *t*-test. Bars represent mean ± s.e.m.

germ-free mice with gut-resident microorganisms. These results place GS in the context of the gut–liver axis, where GS acts as a gatekeeper for methylamine while controling the systemic levels of N^5-methylglutamine. In addition, we showed that cells with high expression of GS derived from brain tumors efficiently synthesize N^5-methylglutamine, demonstrating that the GS-dependent production of N^5-methylglutamine is not unique to specialized hepatocytes. In the brain, GS is highly expressed in astrocytes, and its glutamine-synthesizing activity is essential for glutamatergic neurotransmission, a process where the GS-derived N^5-methylglutamine could play a role.

While the biological effects of N^5-methylglutamine remain to be explored in different physiopathological contexts, we demonstrated that the levels of N^5-methylglutamine are increased in the urine of a β-catenin-mutant genetically engineered mouse model of liver cancer with high GS expression. The levels of N^5-methylglutamine in blood and urine, unlike those of glutamine, are stringent readouts of hepatic GS activity. This finding could lead to the development of a diagnostic tool valuable for GS-expressing WNT/β-catenin-driven HCC, a disease with growing incidence in western society, which currently lacks reliable biomarkers for treatment stratification[31].

Online content

Any methods, additional references, Nature Research reporting summaries, source data, extended data, supplementary information, acknowledgements, peer review information; details of author contributions and competing interests; and statements of data and code availability are available at https://doi.org/10.1038/s41589-022-01154-9.

References

1. Kumada, Y. et al. Evolution of the glutamine synthetase gene, one of the oldest existing and functioning genes. *Proc. Natl Acad. Sci. USA* **90**, 3009–3013 (1993).
2. Elliott, W. H. Adenosinetriphosphate in glutamine synthesis. *Nature* **161**, 128–129 (1948).
3. Eelen, G. et al. Role of glutamine synthetase in angiogenesis beyond glutamine synthesis. *Nature* **561**, 63–69 (2018).
4. Shang, M. et al. Macrophage-derived glutamine boosts satellite cells and muscle regeneration. *Nature* **587**, 626–631 (2020).
5. Bak, L. K., Schousboe, A. & Waagepetersen, H. S. The glutamate/GABA–glutamine cycle: aspects of transport, neurotransmitter homeostasis and ammonia transfer. *J. Neurochem.* **98**, 641–653 (2006).
6. He, Y. et al. Glutamine synthetase deficiency in murine astrocytes results in neonatal death. *Glia* **58**, 741–754 (2010).
7. Häberle, J. et al. Congenital glutamine deficiency with glutamine synthetase mutations. *N. Engl. J. Med.* **353**, 1926–1933 (2005).
8. Qvartskhava, N. et al. Hyperammonemia in gene-targeted mice lacking functional hepatic glutamine synthetase. *Proc. Natl Acad. Sci. USA* **112**, 5521–5526 (2015).
9. Hakvoort, T. B. M. et al. Pivotal role of glutamine synthetase in ammonia detoxification. *Hepatology* **65**, 281–293 (2017).
10. Tardito, S. et al. Glutamine synthetase activity fuels nucleotide biosynthesis and supports growth of glutamine-restricted glioblastoma. *Nat. Cell Biol.* **17**, 1556–1568 (2015).
11. Bott, A. J. et al. Glutamine anabolism plays a critical role in pancreatic cancer by coupling carbon and nitrogen metabolism. *Cell Rep.* **29**, 1287–1298 (2019).
12. Kiourtis, C. et al. Specificity and off-target effects of AAV8-TBG viral vectors for the manipulation of hepatocellular gene expression in mice. *Biol. Open* **10**, bio058678 (2021).
13. Nakai, H. et al. Unrestricted hepatocyte transduction with adeno-associated virus serotype 8 vectors in mice. *J. Virol.* **79**, 214–224 (2005).
14. Roifman, M. et al. Homozygous *GLUL* deletion is embryonically viable and leads to glutamine synthetase deficiency. *Clin. Genet.* **98**, 613–619 (2020).
15. Jang, C. et al. Metabolite exchange between mammalian organs quantified in pigs. *Cell Metab.* **30**, 594–606 (2019).
16. Wellner, V. P., Zoukis, M. & Meister, A. Activity of glutamine synthetase toward the optical isomers of α-aminoadipic acid. *Biochemistry* **5**, 3509–3514 (1966).
17. Zhang, P. et al. Revisiting fragmentation reactions of protonated α-amino acids by high-resolution electrospray ionization tandem mass spectrometry with collision-induced dissociation. *Sci. Rep.* **9**, 6453 (2019).
18. Schubert, H. L., Phillips, J. D. & Hill, C. P. Structures along the catalytic pathway of PrmC/HemK, an N^5-glutamine AdoMet-dependent methyltransferase. *Biochemistry* **42**, 5592–5599 (2003).
19. Levitch, M. E. The demonstration of two discrete enzymes catalyzing the synthesis of glutamine and γ-glutamylmethylamide in *Pseudomonas MS*. *Biochem. Biophys. Res. Commun.* **76**, 609–614 (1977).
20. Barnes, E. M., Zimniak, P. & Jayakumar, A. Role of glutamine synthetase in the uptake and metabolism of methylammonium by *Azotobacter vinelandii*. *J. Bacteriol.* **156**, 752–757 (1983).
21. Golebiewska, A. et al. Patient-derived organoids and orthotopic xenografts of primary and recurrent gliomas represent relevant patient avatars for precision oncology. *Acta Neuropathol.* **140**, 919–949 (2020).
22. Wang, Y. Human PAD4 regulates histone arginine methylation levels via demethylimination. *Science* **306**, 279–283 (2004).
23. Davis, E. J. & De Ropp, R. S. Metabolic origin of urinary methylamine in the rat. *Nature* **190**, 636–637 (1961).
24. Zeisel, S. H., Wishnok, J. S. & Blusztajn, J. K. Formation of methylamines from ingested choline and lecithin. *J. Pharmacol. Exp. Ther.* **225**, 320–324 (1983).
25. Rath, S., Heidrich, B., Pieper, D. H. & Vital, M. Uncovering the trimethylamine-producing bacteria of the human gut microbiota. *Microbiome* **5**, 54 (2017).
26. Cadoret, A. et al. New targets of β-catenin signaling in the liver are involved in the glutamine metabolism. *Oncogene* **21**, 8293–8301 (2002).
27. Dal Bello, B. et al. Glutamine synthetase immunostaining correlates with pathologic features of hepatocellular carcinoma and better survival after radiofrequency thermal ablation. *Clin. Cancer Res.* **16**, 2157–2166 (2010).
28. Huels, D. J. et al. E-cadherin can limit the transforming properties of activating β-catenin mutations. *EMBO J.* **34**, 2321–2333 (2015).
29. Kruspig, B. et al. The ERBB network facilitates KRAS-driven lung tumorigenesis. *Sci. Transl. Med.* **10**, eaao2565 (2018).
30. Losman, J. A., Koivunen, P. & Kaelin, W. G. 2-Oxoglutarate-dependent dioxygenases in cancer. *Nat. Rev. Cancer* **20**, 710–726 (2020).
31. Huang, D. Q., El-Serag, H. B. & Loomba, R. Global epidemiology of NAFLD-related HCC: trends, predictions, risk factors and prevention. *Nat. Rev. Gastroenterol. Hepatol.* **18**, 223–238 (2021).

Methods

Mouse studies

Animal experiments were either subject to review by the University of Ghent Animal Ethics Committee or were performed in accordance with UK Home Office Regulations (project licenses 70/8645 60/4181, PP6345023 and PP0604995) and subject to review by the Animal Welfare and Ethical Review Board of the University of Glasgow. Mice were housed in ventilated cages with ad libitum food and water access and 12-h light/12-h dark cycles. The temperature of the facility was kept between 19 and 23 °C with 55 ± 10% humidity. *Glul*$^{tm3Whla\ fl}$ mice[8] in a C57BL/6 mixed background were kindly provided by M. Mazzone (KU Leuven). *Glul*$^{tm3Whla\ fl}$ mice were bred in-house and were backcrossed (N5–N12) into a C57BL/6J background, and all other mice were on a mixed C57BL/6J background unless otherwise stated. No statistical calculation was done to determine the sample size. Comparable numbers of male and female *Glul*$^{tm3Whla\ fl}$ mice received a single injection of AAV8-TBG-Cre virus (2×10^{11} genomic copies per mouse) at ~60 d of age, and samples were collected at ~120 d of age unless indicated otherwise. Mice heterozygous for *Ctnnb1*$^{lox(ex3)}$ (ref. [28]) received a single injection of AAV8-TBG-Cre virus or AAV8-Null-Cre (2×10^{11} genomic copies per mouse) at 61–71 d of age. After 4 d, the mice were culled, and tissue and blood were sampled. Male and female mice carrying the *Ctnnb1*$^{lox(ex3)/wt}$ and *Rosa26*$^{DM.lsl\text{-}MYC/DM.lsl\text{-}MYC}$,[29] alleles without or with *Glul*$^{tm3Whla\ fl}$ alleles received a single injection of AAV8-TBG-Cre virus (6.4×10^{8} genomic copies per mouse) at ~80 d of age. Triple mutants were backcrossed into C57BL/6J N10. Male mice backcrossed into C57BL/6J N10 carrying the *Rosa26*$^{DM.lsl\text{-}MYC/DM.lsl\text{-}MYC}$ and *Trp53*$^{tm1brn/tm1brn}$ alleles received a single injection of AAV8-TBG-Cre virus (5×10^{10} genomic copies per mouse) at ~57 d of age[32]. Mice were randomly assigned to experimental groups based on their genotypes, and, with the exception of MRI quantification, the analyses were not performed blindly.

Germ-free mice

Axenic 8-week-old C57BL6/J mice from the Ghent Germ-Free and Gnotobiotic Mouse Facility at Ghent University were transferred from flexible film isolators (NKP) to positive-pressure isocages (Tecniplast). Colon and cecum content from one 8-week-old C57BL6/J SPF mouse was isolated under anaerobic conditions and homogenized in 5 ml of sterile PBS with 0.1% L-cysteine. The suspension was left for 5 min to let particulates settle, and the supernatant was transferred to a 50-ml Falcon tube and used as donor material. Five germ-free C57BL6/J mice received an oral gavage with 200 µl of SPF donor microbiota suspension, and six germ-free C57BL6/J mice received an oral gavage with sterile PBS with 0.1% L-cysteine. Both groups were housed in positive-pressure isocages for 3 weeks before mice were killed and tissue was collected.

Stable isotope tracing, methylamine administration and GS inhibition in vivo

Wt/wt and Δ/Δ mice were injected intraperitoneally (IP) with 2 g per kg (body weight) U-$^{13}C_6$ glucose (CLM-1396, Cambridge Isotopes) or 2 mmol per kg (body weight) ^{13}C-methylamine (277630, Sigma-Aldrich), and tissue samples were collected 30 min and 2 h after injections, respectively. Wt/wt mice were IP injected with 200 mg per kg (body weight) U-$^{13}C_5$-glutamine (CLM-1822, Cambridge Isotopes). Shortly before injection, blood was collected by tail vain puncture and immediately diluted 1:50 in the extraction solution for LC–MS analysis. Thirty minutes after injection, mice were killed, and blood was collected by cardiac puncture and processed as described above. Methylamine (426466, Sigma-Aldrich) was supplemented in the drinking water (0.1% (wt/vol)) to 6- to 9-week-old wt/wt and Δ/Δ mice for 5 months. Water consumption was not affected by methylamine supplementation, and age-matched mice not administered methylamine were used as controls.

Six- to 9-week-old wt/wt mice were injected IP either with NaCl 0.9% (vehicle solution) or 10 mg per kg (body weight) MSO (M5379, Sigma-Aldrich). Blood was collected by tail vain puncture shortly before (0 h) and 2, 4, 8 and 24 h after MSO injection and immediately diluted 1:50 in the extraction solution for LC–MS analysis. Tissue samples were collected for analysis 4 h after MSO administration.

MALDI imaging

Serial sections of wt/wt and Δ/Δ livers were cut at 10-µm thickness, processed for standard immunohistochemistry (IHC) for GS and OAT or mounted on IntelliSlides (1868957, Bruker) for MALDI imaging. Sections from wt/wt and Δ/Δ livers were paired on each slide. Freeze-dried sections were shipped to the Bruker Daltonics facilities and sprayed with *N*-(1-naphthyl)-ethylenediamine dihydrochloride matrix with a TM-sprayer (HTX Technologies). Data were acquired on a timsTOF fleX instrument (Bruker) in negative Q-TOF ion mode at a 10-µm pixel size. Metabolic compounds were automatically annotated using MetaboScape 2021b (Bruker), and ion distributions were visualized with SCiLS Lab 2021c (Bruker).

Magnetic resonance imaging and urine collection

At 121–156 d after AAV8-TBG-Cre administration, urine samples were collected from *Cnntb1*$^{lox(ex3)/wt}$*Rosa26*$^{DM.lsl\text{-}MYC/DM.lsl\text{-}MYC}$ mice and immediately diluted 1:50 in LC–MS extraction solution. Within 24 h of urine collection, MRI images were acquired on a nanoScan PET/MRI (Mediso) using the 35-mm radiofrequency coil. A non-gated T1-weighted gradient echo sequence in the coronal/sagittal plane was acquired in three dimensions with a repetition time of 20 ms, echo time of 3.8 ms and flip angle of 15°. The image matrix is non-isotropic with dimensions of 179 × 512 × 60 and a field of view of 3.58 × 10.24 × 3.00 cm. Standard Fourier transform was used for reconstruction. No postprocessing was performed, and manual segmentation was performed blindly using VivoQuant ver4.0 (Invicro).

Cell lines

HEK293 and HepG2 cell lines were obtained from ATCC. T16 cells were kindly provided by S. Niclou (Luxembourg Institute of Health). HEK293 and HepG2 cells were routinely cultured with MEM with 1 g liter^{-1} glucose (21090022, Gibco) supplemented with 2 mM glutamine (Gibco), 1% non-essential amino acids (11140035, Gibco), 1 mM pyruvate (S8636, Sigma-Aldrich) and 10% FBS (10270106, Gibco). T16 cells were routinely cultured in MEM (21090022, Gibco) supplemented with 1% non-essential amino acids (11140035, Gibco), 0.65 mM glutamine (A2916801, Gibco), 0.1 mM pyruvate (S8636, Sigma-Aldrich), 1% ITS (1 g liter^{-1} insulin, 550 mg liter^{-1} transferrin, 670 µg liter^{-1} sodium selenite; 41400045, Gibco), 10 ng ml^{-1} epidermal growth factor (EGF; AF-100-15, Peprotech), 10 ng ml^{-1} fibroblast growth factor (FGF; AF-100-18B, Peprotech), 6.8 µg ml^{-1} vitamin B12 (V6629, Sigma-Aldrich), 2 µg ml^{-1} heparin (H3393, Sigma-Aldrich) and 400 mg liter^{-1} AlbuMAX II (11021029, Thermo Fisher Scientific). For the experiments with HEK293 and HepG2 cell lines, cells were seeded in complete MEM, and 15–24 h later, the medium was replaced with Plasmax[33] supplemented with 2.5% FBS (10270106, Gibco) and 200 mg liter^{-1} AlbuMAX II (11021029, Thermo Fisher Scientific) for an additional 24 h before the experiments. For the experiments, T16 cells were cultured in Plasmax[33] supplemented with AlbuMAX II (11020029, Thermo Fisher Scientific), ITS, FGF, EGF and heparin at the concentrations used for routine culture. All cell lines were authenticated using the Promega GenePrint 10 kit (B9510, Promega) and tested negative for mycoplasma infection using the MycoAlert mycoplasma detection kit (LT07-318, Lonza).

CRISPR–Cas9 and overexpression constructs

Non-targeting control sequence and two guide RNAs (gRNAs) against exon 3 of *GLUL* were cloned into LentiCRISPRv2 (refs. [34,35]) using BsmBI restriction enzyme. For each sequence, 3×10^5 HepG2 or HEK293 cells were transfected with 1 µg of gRNA using jetPrime (Polyplus). Twenty-four hours after transfection, the media were

replaced and supplemented with 1 μg ml^{-1} puromycin for selection. Puromycin-resistant cells (500) were seeded in a 25-cm cell culture dish. Individual clones were collected, and GS expression was tested by immunoblotting. The following gRNA target sequences were used: non-targeting control gRNA, 5′-GTAGCGAACGTGTCCGGCGT-3′; *GLUL* gRNA 1, 5′-TCTGTAGGTCCATATTACTG-3′; *GLUL* gRNA 2, 5′-TTCTAGTGGGAATTTCAGAT-3′. The plasmids containing wt, R324A and R324C *GLUL* cDNA were kindly provided by U. Kutay (ETH Zurich)[36]. The *GLUL* coding sequence was subcloned from pcDNA5/FRT/TO/HA into pcDNA3.1 NEO (+) using 5′-BamHI and 3′-EcoRI restriction sites. However, these vectors lack the Kozak sequence upstream of the start codon of *GLUL*, which is required for efficient translation of the full-length GS protein. To add the wt Kozak sequence to the *GLUL* expression cassette, the plasmids were linearized by BamHI and BsrGI digestion, and a repair oligonucleotide was ligated into the plasmid. These repair oligonucleotides contain the sequence for five nucleotides upstream of the *GLUL* start codon (5′-CCACCATG-3′). The sense sequence was

5′-ATCCACCATGACCACCTCAGCAAGTTCCCACTTAAATAAAGGCATCAAGCAGGT-3′, and the antisense sequence was

5′-GTACACCTGCTTGATGCCTTTATTTAAGTGGGAACTTGCTGAGGTGGTCATGGTG-3′. *GLUL* sequences were confirmed by Sanger sequencing.

Enzymatic assays

Enzymatic assays were performed using a modified protocol described previously[37,38]. Briefly, 2 μg of human recombinant GS obtained from Novus Biologicals (NBP2-52376) or purified GS obtained as described in the next section was added to the reaction mixture consisting of 100 mM imidazole/HCl (pH 7.2; I5513, Sigma-Aldrich), 50 mM glutamate (pH 7.2; G5889, Sigma-Aldrich), 20 mM ATP (pH 7.2; A7699, Sigma-Aldrich) and 20 mM $MgCl_2$ (M4880, Sigma-Aldrich). Unless otherwise indicated, 500 μl of reaction mixture was incubated for 2 min at 37 °C, and the reaction was initiated by adding NH_4Cl (A9434, Sigma-Aldrich), CH_3NH_2·HCl (M0505, Sigma-Aldrich), $^{15}NH_4Cl$ (299251, Sigma-Aldrich) or ^{13}C-methylamine (277630, Sigma-Aldrich) at the concentrations indicated in Fig. 4f,g or in the legends of Extended Data Fig. 3a,b. Aliquots (5 μl) of the reaction mixtures were sampled at the times specified in the figure legends, diluted 1:1,000 in LC–MS extraction solution and analyzed by LC–MS. K_m values were calculated in GraphPad 9.4 (Prism) by using a Michaelis–Menten equation. N^2-Methyl-L-glutamine used in Fig. 2j was synthesized by replacing glutamate with 40 mM *N*-methyl-L-glutamate (ICN15555583, Fisher Scientific) in the reaction mixture described above. The reaction was incubated at 37 °C for 2 h, and an aliquot of the mixture was diluted 1:1,000 for LC–MS/MS analysis.

Expression and purification of human wt GS and R324C mutant

Full-length human *GLUL* wt and R324C mutant were amplified using 5′ primer (5′-TAAGCAGGATCCACCACCTCAGCAAGTTCCCACTTAAATAAAGGC-3′) with BamHI and 3′ primer (5′- TGCTTAGAATTCTTAATTTTTGTACTGGAAGGGCTCATCGCCGG-3′) with EcoRI from pCDNA3.1 GS–HA. Following double digestion and agarose gel purification, *GLUL* fragments were ligated into pRSF-DUET containing 12×His-SUMO, and the sequence was confirmed with Sanger sequencing. Chemically competent *Escherichia coli* BL21(DE3) Rosetta2 pLysS (Novagen) cells were transformed with 12×His-SUMO–GS in pRSF-DUET. Cell cultures were grown in Luria–Bertani medium supplemented with 1 mM $MgSO_4$ at 37 °C to an optical density at 600 nm of ~0.8 and induced with 0.35 mM isopropyl β-D-1-thiogalactopyranoside; expression occurred overnight at 16 °C. Cells were collected, centrifuged (600*g*), resuspended in IMAC buffer A (25 mM sodium phosphate, 500 mM NaCl and 50 mM imidazole, pH 7.5) and lysed with a microfluidizer at 10,000 psi. The lysate was cleared by spinning at 19,000 r.p.m. for 45 min at 4 °C, syringe filtered using a 0.45-μm filter and loaded onto a 5-ml His-Trap HP column (GE Life Sciences). The loaded column was washed for 30 column volumes (cv) in IMAC buffer A and eluted with 100% IMAC buffer B (25 mM sodium phosphate, 500 mM NaCl and 350 mM imidazole, pH 7.5) for 5 cv. Fractions were combined and dialyzed against ULP1 cleavage buffer (25 mM Tris, 500 mM NaCl and 5 mM β-mercaptoethanol, pH 8.0) overnight at 4 °C in 3,500 molecular weight cutoff (MWCO) SnakeSkin dialysis tubing (Thermo Fisher) with 5 μM SUMO protease (ULP1). The cleavage reaction was filtered using a 0.45-μm syringe filter and pass backed over a 15-ml His-Trap HP column (GE Life Sciences). The flowthrough was concentrated in a 10,000-MWCO Amicon centrifugal filter unit (Merck Millipore) to a final volume of 3 ml and loaded on a 26/600 Superdex 200 SEC column (GE Life Sciences) preequilibrated in SEC buffer (20 mM HEPES, 300 mM NaCl and 0.5 mM TCEP, pH 7.5). Full-length GS eluted ~0.59 cv, and pure fractions confirmed by SDS–PAGE were concentrated to 67–117 μM using a 10,000-MWCO Amicon centrifugal filter unit. Protein aliquots were stored at −80 °C until use.

LC–MS metabolomics

Cells were extracted as previously described[33]. Briefly, cells plated in six wells were washed three times with ice-cold PBS and incubated for 5 min at 4 °C with 400 μl of LC–MS extraction solution (20% water, 50% methanol and 30% acetonitrile).

Tissue fragments (20–40 mg) were extracted by using the Precellys Evolution homogenizer (Bertin) and 25 μl of LC–MS extraction solution per mg of tissue. Cell and tissue extracts were centrifuged at 16,000*g* for 10 min at 4 °C, and the supernatant was stored at −74 °C until LC–MS analysis. Compound peak areas obtained for cells were normalized on the total micrograms of proteins determined for each extracted well with a modified Lowry assay[33].

Metabolites from the biological extracts were injected (5 μl) and separated using a ZIC-pHILIC column (SeQuant; 150 mm × 2.1 mm, 5 μm; Merck) coupled with a ZIC-pHILIC guard column (SeQuant; 20 mm × 2.1 mm) using an Ultimate 3000 HPLC system (Thermo Fisher Scientific). Chromatographic separation was performed using a 15-min linear gradient starting with 20% ammonium carbonate (20 mM, pH 9.2) and 80% acetonitrile, terminating at 20% acetonitrile at a constant flow rate of 200 μl min^{-1}. The column temperature was held at 45 °C.

A Q Exactive Orbitrap mass spectrometer (Thermo Fisher Scientific) equipped with electrospray ionization was coupled to the HPLC system for both metabolite profiling and metabolite identification. For profiling, the polarity switching mode was used with a resolution (RES) of 35,000 or 70,000 at 200 *m*/*z* to enable both positive and negative ions to be detected across a mass range of 75 to 1,000 *m*/*z* (automatic gain control (AGC) target of 1×10^6 and maximal injection time (IT) of 250 ms).

Data-dependent fragmentation was performed to aid metabolite identification using a wt/wt liver pooled sample comprised of a mixture of all sample extracts analyzed per experimental batch. The Q Exactive was operated in positive and negative polarity mode separately (35,000 RES, AGC target of 1×10^6 and max IT of 100 ms), and the ten most abundant ions were chosen for fragmentation (minimum AGC target of 1×10^3, AGC target of 1×10^5, max IT of 100 ms, 17,500 RES, stepped normalized collision energy of 25, 60 and 95, isolation width of 1 *m*/*z*, dynamic exclusion of 15 s and charge exclusion of >2) per survey scan.

Data-independent fragmentation was performed to acquire fragmentation spectra of specific metabolites including 5-methylglutamine (positive polarity, *m*/*z* 161.0920). Fragmentation spectra were continuously recorded with the following parameters: 17,500 RES, isolation width of 0.7 *m*/*z*, AGC target of 1×10^5, max IT of 250 ms and stepped normalized collision energy of 25, 60 and 95.

Untargeted metabolomics analysis was performed using Compound Discoverer software (Thermo Scientific v3.2). Retention times were aligned across all data files (maximum shift of 2 min and mass

tolerance of 5 ppm). Unknown compound detection (minimum peak intensity of 1×10^6) and grouping of compounds were performed across all samples (mass tolerance of 5 ppm and retention time tolerance of 0.7 min). Missing values were filled using the software's 'Fill Gap' feature (mass tolerance of 5 ppm and signal/noise tolerance of 1.5). Compound identification was assigned by matching the mass and retention time of observed peaks to an in-house library generated using metabolite standards (mass tolerance of 5 ppm and retention time tolerance of 0.5 min) or by matching fragmentation spectra to mzCloud (www.mzcloud.org; precursor and fragment mass tolerance of 10 ppm and match factor threshold of 60).

Targeted metabolomics analysis was performed using Tracefinderv4.1 (Thermo Scientific), and the peak areas of metabolites were determined by using the *m/z* of the singly charged ions (extracted ion chromatogram, ±5 ppm) and the retention time from our in-house metabolite library.

N^5-Methylglutamine was quantified in the serum and urine samples by a standard addition method. The concentrations of D,L-N^5-methylglutamine indicated in Extended Data Fig. 4h, m–o were obtained by spiking a stock solution of the compound to a solution extracted and pooled from the respective fluid samples ($n = 4$ mice for serum and $n = 5$ mice for urine). The same method was used to quantify N^5-methylglutamine in wt/wt liver samples ($n = 1$) spiked with D,L-N^5-methylglutamine to obtain final concentrations of 0, 1, 5, 10 and 20 µM. To estimate the micromolar concentration of N^5-methylglutamine in liver tissue, we used a ratio of 1 mg of wet tissue per µl. The samples used for the quantification of serum concentrations were analyzed with the Q Exactive operated in positive-selective ion monitoring mode (70,000 RES, AGC target of 2×10^5, max IT of 240 ms and *m/z* of 161.0919 ± isolation window of 1 *m/z*) using the same chromatographic conditions as above. All other samples were analyzed as described above for biological extracts.

Methylamine was quantified with an LC–MS method adapted from previous reports[39,40]. An aliquot of 25 µl of mouse serum was transferred to an Eppendorf tube, and 5 µl of trichloroacetic acid (20% in water) was added and mixed by vortexing for 30 s. The samples were centrifuged at 12,000*g* for 10 min, and 15 µl of the supernatant was transferred to a new tube and supplemented with 22.5 µl of borate buffer (0.5 M, pH 11) and 12.5 µl of tosyl chloride (10 mg ml^{-1} in acetonitrile). The mixture was mixed by vortexing for 5 s and incubated for 2 h at 50 °C. The samples were cooled down at room temperature and analyzed by LC–MS. A selected reaction monitoring mode was used to detect derivatized methylamine on an Altis QQQ mass spectrometer equipped with a Vanquish LC system (Thermo Fisher Scientific). Chromatography was performed on an Acquity HSS T3 column (Waters; 150 mm × 2.1 mm, 1.8 µm). The mobile phase consisted of solvent A (water with 0.1% formic acid) and solvent B (acetonitrile with 0.1% formic acid). Separation of metabolites was performed with the following gradient: 0 min 20% B, 8 min 95% B and 10 min 20% B at a constant flow rate of 0.3 ml min^{-1}. The injection volume was 5 µl. Three transitions were optimized using a standard of derivatized methylamine from the positive precursor ion (*m/z* 185.9) to product ions (*m/z* 64.8, 90.8 and *m/z* 154.9). The total cycle time was 0.8 s, and Q1 RES was (full-width at half-maximum) 0.7 and Q3 RES was (full-width at half-maximum) 1.2. For each transition, the collision energy applied was optimized to generate the greatest possible signal intensity and using the calibrated RF values. The optimized source parameters were a spray voltage of 3,500 V, sheath gas of 35, aux gas of 7, ion transfer tube temperature of 325 °C and vaporizer temperature of 275 °C. Data acquisition was performed using Xcalibur 4.1 (Thermo Scientific) software, and quantification was performed using Tracefinderv4.1 (Thermo Scientific).

Ammonia measurement

Ammonia concentration was measured in frozen sera or in blood collected from the tail vein of mice and immediately analyzed with the blood ammonia meter PocketChem BA PA-4140 (Arkray).

Immunohistochemistry

Tissue samples were fixed in a 10% solution of neutral buffered formalin overnight (16–24 h) and transferred to 70% ethanol. Paraffin-embedded tissue blocks were cut into 5-µm sections and stained with hematoxylin and eosin or with the following antibodies: GS (1:800; HPA007316, Sigma-Aldrich) and OAT (1:200; ab137679, Abcam). IHC images were visualized with an Aperio ImageScope v12.4 (Leica Biosystems).

Immunoblotting

Cells were washed twice with ice-cold PBS, and proteins were extracted with RIPA buffer (20-188, EMD Millipore) containing protease and phosphatase inhibitors (A32961, Thermo Fisher Scientific). Protein amounts were quantified with a standard bicinchoninic acid assay (A32961, Pierce). Tissues were extracted with 25 µl of RIPA buffer per mg of wet weight. Tissue fragments were homogenized with the Precellys Evolution homogenizer (Bertin), and 20–80 µg of protein extract was loaded in 9.5% acrylamide gels for electrophoresis and blotted onto nitrocellulose membranes. PageRuler prestained protein ladder (26616, Thermo Fisher Scientific) was used as a reference for the protein molecular weight. Membranes were incubated overnight with the following primary antibodies: GS (1:1,000; 610517, BD Bioscience), OAT (1:1,000; ab137679, Abcam), β-actin (1:1,000; ab8229, Abcam), β-tubulin (1:2,000; T5201, Sigma-Aldrich) and vinculin (1:1,000; V9131, Sigma-Aldrich). The secondary antibodies anti-rabbit horseradish peroxidase (1:1,000; 7074, Cell Signaling Technology), anti-mouse IRDye 800CW (1:2,500; 926-32212, Licor) and anti-goat IRDye 680CW (1:2,500; 926-68074, Licor) were used, and membranes were imaged with an Odyssey infrared scanner and visualized with Image Studio Lite 5.2 (Licor) or imaged with Clarity Western ECL substrate (1705061, Bio-Rad) and a Chemidoc MP imager (Bio-Rad) and visualized with Chemidoc Image Lab 6.0 (Bio-Rad). Scanned images of uncropped membranes are shown in the Source Data.

Reporting summary

Further information on research design is available in the Nature Research Reporting Summary linked to this article.

Data availability

All the data supporting the findings of this study are available within the article. Source data files that support the findings of this study are stored at the Cancer Research UK Beatson Institute and are available from the corresponding author upon reasonable request. Requests for unique biological materials can be made to the corresponding author. Source data are provided with this paper.

References

32. Müller, M. et al. Human-correlated genetic HCC models identify combination therapy for precision medicine. Preprint at *Research Square* https://doi.org/10.21203/rs.3.rs-1638504/v1 (2022).
33. Vande Voorde, J. et al. Improving the metabolic fidelity of cancer models with a physiological cell culture medium. *Sci. Adv.* **5**, eaau7314 (2019).
34. Sanjana, N. E., Shalem, O. & Zhang, F. Improved vectors and genome-wide libraries for CRISPR screening HHS public access supplementary material. *Nat. Methods* **11**, 783–784 (2014).
35. Shalem, O. et al. Genome-scale CRISPR–Cas9 knockout screening in human cells. *Science* **343**, 84–87 (2014).
36. Badertscher, L. et al. Genome-wide RNAi screening identifies protein modules required for 40S subunit synthesis in human cells. *Cell Rep.* **13**, 2879–2891 (2015).
37. Wellner, V. P. & Meister, A. Binding of adenosine triphosphate and adenosine diphosphate by glutamine synthetase. *Biochemistry* **5**, 872–879 (1966).

38. Listrom, C. D. et al. Expression, purification, and characterization of recombinant human glutamine synthetase. *Biochem. J.* **328**, 159–163 (1997).
39. Li, H., Luo, W., Lin, J., Lin, Z. & Zhang, Y. Assay of plasma semicarbazide-sensitive amine oxidase and determination of its endogenous substrate methylamine by liquid chromatography. *J. Chromatogr. B Analyt. Technol. Biomed. Life Sci.* **810**, 277–282 (2004).
40. Nalazek-Rudnicka, K. & Wasik, A. Development and validation of an LC–MS/MS method for the determination of biogenic amines in wines and beers. *Monatsh. Chem.* **148**, 1685–1696 (2017).

Acknowledgements

We thank the Core Services and Advanced Technologies at the Cancer Research UK Beatson Institute (C596/A17196 and A31287) and particularly the Metabolomics, Translational Molecular Imaging, Biological Services Unit, Histology Service and Molecular Technologies. We acknowledge M. Mazzone (KU Leuven) for providing the mice carrying the *Glul*$^{tm3Whla\ fl}$ allele, U. Kutay (ETH Zurich) for providing the *GLUL* pcDNA/FRT/TOcHA (wt, R324A, R324C) plasmids, J.P. Morton for providing the KPC mice and S. Niclou (Luxembourg Institute of Health) for providing the T16 glioblastoma cells. We acknowledge C. Winchester for comments on the manuscript and all members of the Oncometabolism laboratory and the Metabolomics Facility for constructive discussions. This work was funded by Cancer Research UK awards A17196 and A31287 (CRUK Beatson Institute), Cancer Research UK RadNet Glasgow Centre award A28803 (A.B.), Wellcome Trust grant WT107492Z (T.G.B. and M.M.), Cancer Research UK HUNTER accelerator award A26813 (E.H.T.), Cancer Research UK award A25045 and DRCQQR-May21\100002 (O.J.S.), Cancer Research UK award A29256 (D.T.H.), Cancer Research UK award A29799 (K.B.), Cancer Research UK award A25006 (D.Y.L.) and Cancer Research UK award A23982 (S.T.).

Author contributions

The study was conceptualized by V.H.V., D.S., K.B. and S.T. Methods were developed by D.S., M.M., T.A., M.A.N., T.G.B., D.J.M., J.O., L.V. and A.B. Experiments were performed by V.H.V., M.F.A., R.D., D.S., T.M.D., E.H.T., S.M., M.M., J.V.V., M.J., G.B. and C.N. Data were graphically visualized by V.H.V. and S.T. The study was supervised by T.G.B., D.Y.L., D.T.H., K.B., O.J.S. and S.T. The manuscript was written by V.H.V. and S.T., with reviewing and editing by T.G.B., T.M.D., D.J.M., J.V.V., O.J.S. and K.B. Funding was acquired by A.B., T.G.B., M.M., E.H.T., D.T.H., D.Y.L., K.B., O.J.S. and S.T.

Competing interests

J.O. is employed at Bruker Daltonics GmbH & Co. KG. All other authors declare no competing interests.

Additional information

Extended data is available for this paper at https://doi.org/10.1038/s41589-022-01154-9.

Supplementary information The online version contains supplementary material available at https://doi.org/10.1038/s41589-022-01154-9.

Correspondence and requests for materials should be addressed to Saverio Tardito.

Peer review information *Nature Chemical Biology* thanks Jing Fan and the other, anonymous, reviewer(s) for their contribution to the peer review of this work.

Reprints and permissions information is available at www.nature.com/reprints.

https://doi.org/10.1038/s41589-022-01154-9

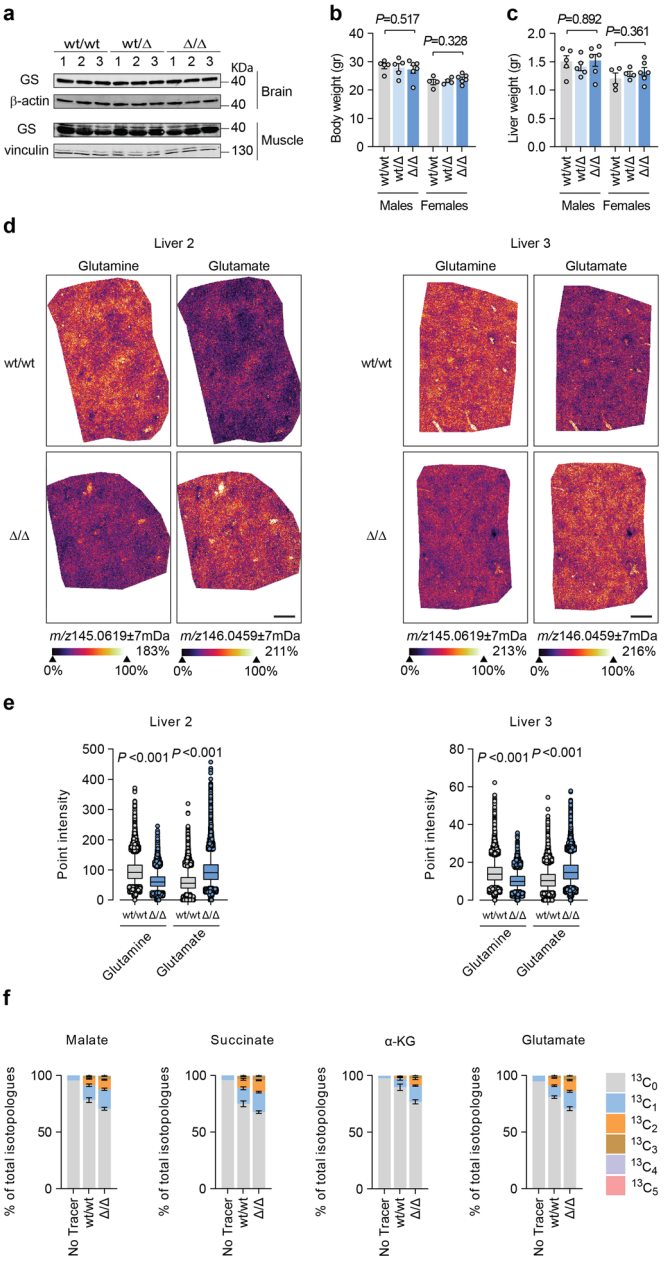

Extended Data Fig. 1 | Metabolic effects of hepatic GS deletion. a, Immunoblot for GS of brain (top) and muscle (bottom) samples from wt/wt (n = 3), wt/Δ (n = 3), Δ/Δ (n = 3) mice shown in Fig. 1d. β-actin and vinculin are shown as loading controls. **b**, Body weights and (**c**) liver weights of male wt/wt (n = 5), wt/Δ (n = 5), Δ/Δ (n = 6) and female wt/wt (n = 4), wt/Δ (n = 4), Δ/Δ (n = 6) mice. Two-tailed Student's t-test. Bars are mean ± s.e.m. **d**, Glutamine and glutamate relative abundance is shown in sections of frozen liver samples from wt/wt (n = 1 male, n = 1 female) and Δ/Δ mice (n = 1 male, n = 1 female) analyzed with mass spectrometry metabolic imaging. Data were normalized with root mean square method. Scale bar = 1 mm. **e**, Glutamine and glutamate quantification of the metabolic images presented in (d) (n = 2 wt/wt, n = 2 Δ/Δ). Each box and whiskers represents data from one image obtained from one liver. Box with bounds at 25th-75th percentiles, line at median, and whiskers at 5th-95th percentiles, each data point represents the relative intensity of one pixel. Two-tailed Student's t-test. **f**, Relative levels of ^{13}C isotopologues for the indicated metabolites in the liver extracts of a no tracer control mouse (n = 1) and in wt/wt (n = 4) and Δ/Δ (n = 5) mice administered with U-$^{13}C_6$-glucose. Bars are mean ± s.e.m.

https://doi.org/10.1038/s41589-022-01154-9

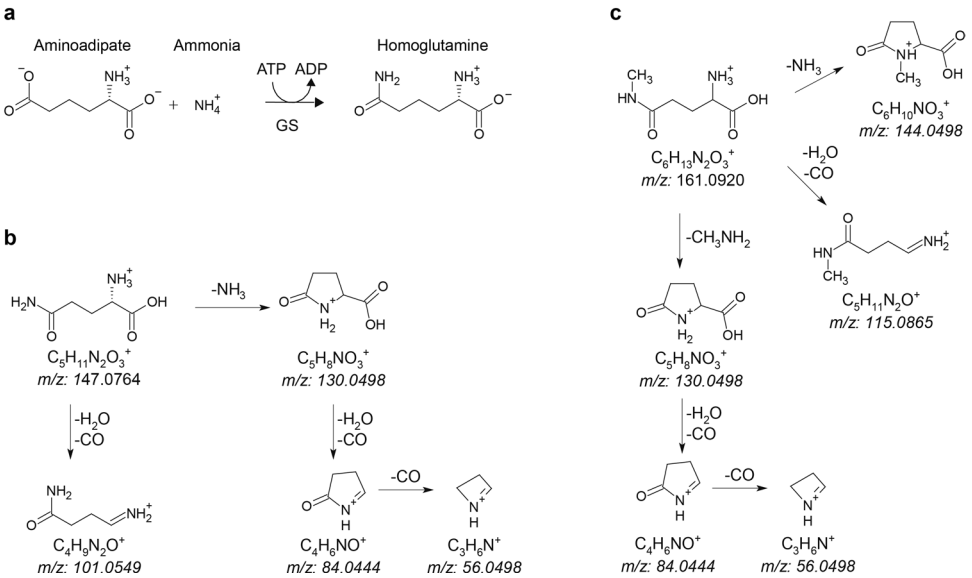

Extended Data Fig. 2 | Proposed mechanisms of reaction and fragmentation. a, Schematic of the proposed reaction where α-aminoadipic acid and ammonia are used by GS to produce homoglutamine[16]. **b**, Proposed mechanism for glutamine fragmentation[17]. **c**, Proposed mechanism for N5-methylglutamine fragmentation.

https://doi.org/10.1038/s41589-022-01154-9

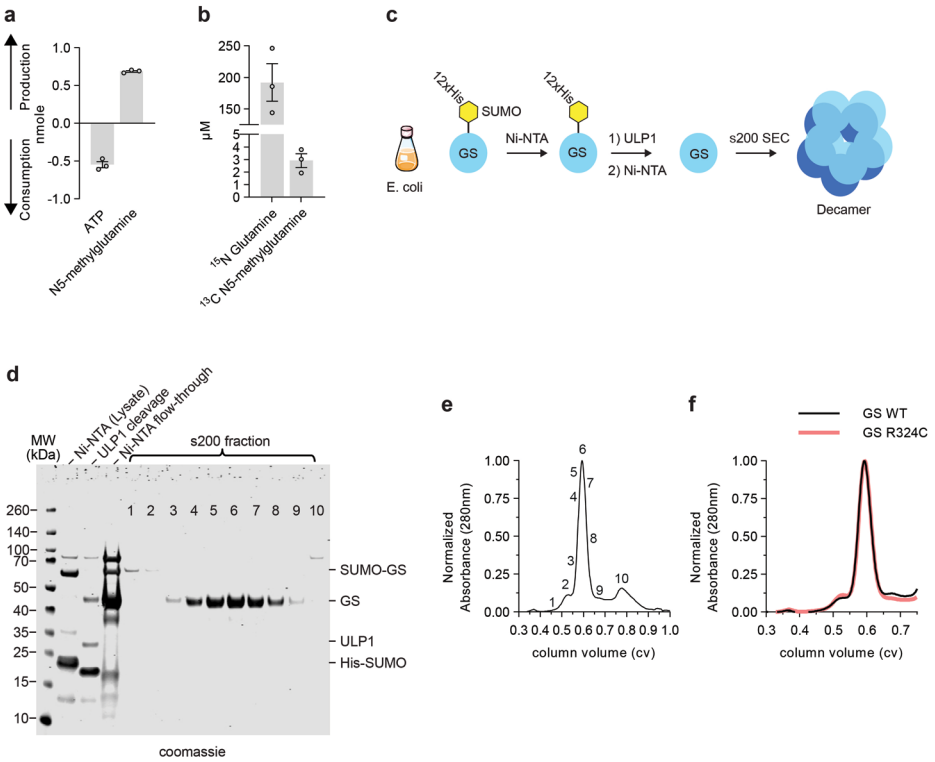

Extended Data Fig. 3 | Stoichiometry of GS activities and purification of GS wild type and R324C mutant proteins. a, Recombinant human GS protein was incubated in 50 µl of the reaction mixture described in the methods section with 40 mM methylamine. The differences in nanomoles of ATP and N5-methylglutamine between samples harvested before and 60 minutes after methylamine addition are shown. Each data point represents an independent experiment (n = 3). Bars are mean ± s.e.m.. **b**, Recombinant human GS protein was incubated in 500 µl of the reaction mixture described in the Methods section. The reaction was started by adding a solution containing 20 mM ^{13}C methylamine and 20 mM ^{15}N ammonia. ^{13}C N5-methylglutamine and ^{15}N glutamine were quantified in samples harvested 60 minutes after the reaction start. Each data point represents an independent experiment (n = 3). Bars are mean ± s.e.m.. **c**, Schematic of the purification steps for GS WT and GS R324C described in the Methods section. **d**, Coomassie stained SDS$^-$PAGE gel showing the purification steps and size exclusion fractions for GS WT protein. SDS-PAGE gels for the purification of GS WT and GS R324C showed comparable results (n = 1). **e**, Superdex 200 size exclusion profile for the GS WT protein. **f**, Overlay of size exclusion profiles for GS WT and GS R324C loaded separately onto a Superdex 200 column. The elution profiles were overlaid demonstrating an identical oligomeric state for GS WT and mutant.

https://doi.org/10.1038/s41589-022-01154-9

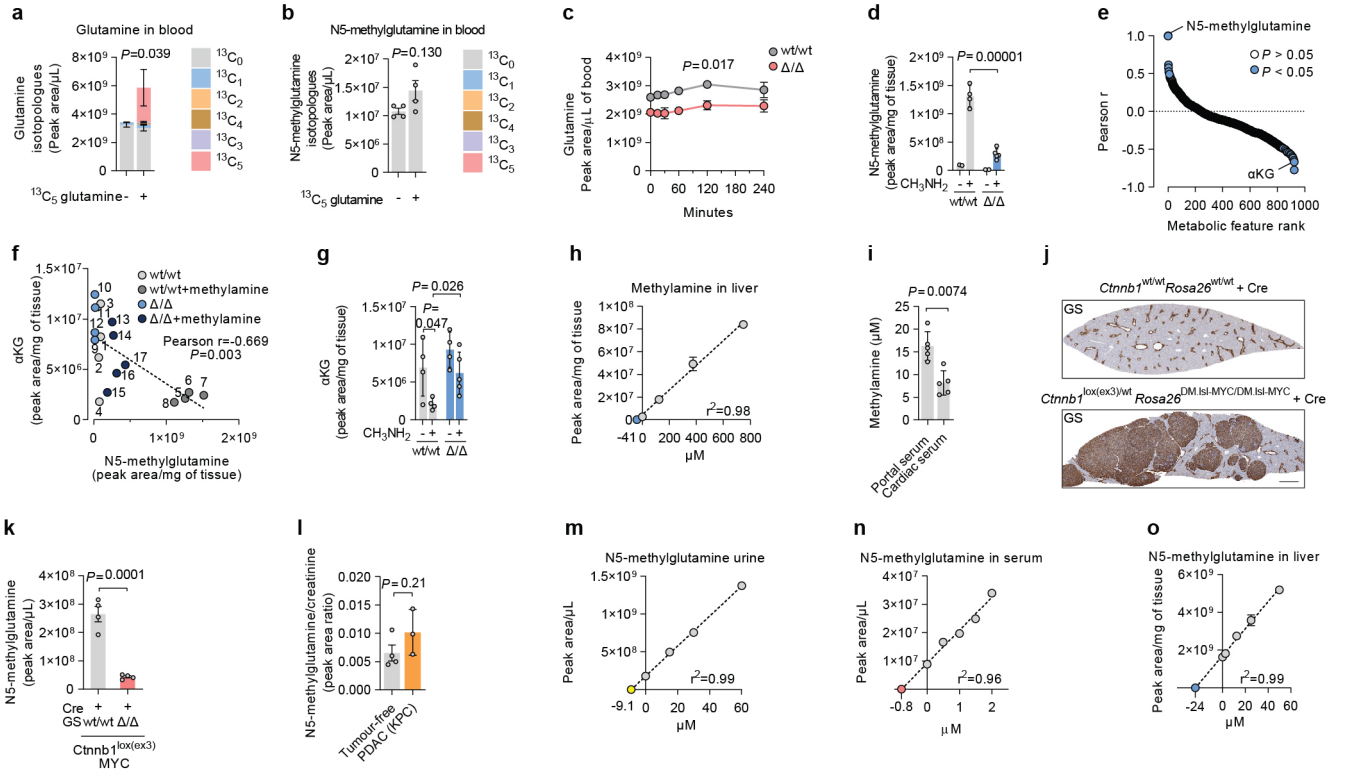

Extended Data Fig. 4 | N5-methylglutamine *in vivo* metabolic origin, its effects on liver metabolism, and its levels in murine cancer models. **a**, **b**, Glutamine and N5-methylglutamine isotopologue levels in the blood of wt/wt mice (n = 4, 2 females and 2 males) before (-) and after (+) administration of $^{13}C_5$ glutamine. *P* values refer to the sum of all detected isotopologues. Two-tailed ratio paired Student's t-test. Bars are mean ± s.e.m.. **c**, Levels of glutamine in the blood of wt/wt (n = 3) and Δ/Δ (n = 3) mice injected with ^{13}C methylamine. *P* value refers to the comparison of wt/wt to Δ/Δ blood at 120 minutes. Two-tailed Student's t-test. Circles are mean ± s.e.m.. **d**, N5-methylglutamine levels in the liver tissue of wt/wt (n = 4, 3 females and 1 male) and Δ/Δ (n = 5, 3 females and 2 males) mice administered 0.1% w/v methylamine, supplemented to drinking water for 5 months, or in wt/wt (n = 4, 2 females and 2 males) and Δ/Δ (n = 4, 3 females and 1 male) control mice. Two-tailed Student's t-test. Bars are mean ± s.e.m.. **e**, Metabolic features identified by untargeted metabolomic analysis of liver tissue of the mice described in (d) and ranked according to their correlation values with N5-methylglutamine levels shown in (d) (n = 4 wt/wt and n = 5 Δ/Δ administered methylamine, n = 4 wt/wt and n = 4 Δ/Δ with water control). Cut-off *P* values refers to a two tailed Pearson correlation analysis (n = 17). **f**, Two tailed Pearson correlation analysis (n = 17) between the α-ketoglutarate and N5-methylglutamine in the liver tissues of mice described in (d). **g**, α-ketoglutarate levels in liver tissue of the mice described in (d). n = 4 wt/wt and n = 5 Δ/Δ administered methylamine, n = 4 wt/wt and n = 4 Δ/Δ with water control. Two-tailed Student's t-test. Bars are mean ± s.e.m.. **h**, Methylamine concentrations quantified with a standard addition method in liver tissue (n = 1) assuming that 1 g of tissue = 1 ml. Circles are mean ± s.e.m. of 2 technical replicates. **i**, Methylamine concentrations in portal and cardiac sera. Wild type C57Bl6/J mice were fasted overnight for 16 hours and refed for 4 hours (post-absorptive state) before being anesthetized. For each mouse samples of blood were collected by venipuncture from the portal vein and subsequently by cardiac puncture (n = 5 mice). Two-tailed ratio paired Student's t-test. Data are mean ± s.e.m.. **j**, Images of IHC staining for GS in liver sections from *Ctnnb1*$^{wt/wt}$, *Rosa26*$^{wt/wt}$ or *Ctnnb1*$^{lox(ex3)/wt}$, *Rosa26*$^{DM.lsl\text{-}MYC/DM.lsl\text{-}MYC}$ female mice, harvested 107 and 151 days after administration of AAV8-TBG-Cre. Scale bar = 1 mm. The images shown are representative of 3 mice per genotype. **k**, Levels of N5-methylglutamine in the serum sampled at clinical endpoint from tumour-bearing *Ctnnb1*$^{lox(ex3)/wt}$, *Rosa26*$^{DM.lsl\text{-}MYC/DM.lsl\text{-}MYC}$ male mice with GS wt/wt (n = 4) or GS Δ/Δ (n = 4), described in Fig. 6e. Two-tailed Student's t-test. Bars are mean ± s.e.m.. **l**, Normalized urine levels of N5-methylglutamine from tumour-free mice described in Fig. 6e (n = 4) and from K-ras$^{LSL.G12D/+}$, Trp53$^{R172H/+}$, Pdx-1-Cre (KPC) mice with pancreatic ductal adenocarcinoma (PDAC) sampled at clinical endpoint (n = 3). Two-tailed Student's t-test. Bars are mean ± s.e.m.. **m**-**o**, N5-methylglutamine concentrations quantified with a standard addition method in urine (m) (n = 1, pooled urine from 5 mice), serum (n) (n = 1 pooled sera from 4 mice), and liver tissue (o) (assuming that 1 g of tissue =1 ml, n = 1). Coloured circles indicate the x intercept, and their absolute values correspond to the µM concentrations of metabolites in the samples without standard addition. Circles are mean ± s.e.m. of 2 (m, o) or 3 (n) technical replicates.

nature portfolio

Corresponding author(s): Saverio Tardito

Last updated by author(s): Aug 18, 2022

Reporting Summary

Nature Portfolio wishes to improve the reproducibility of the work that we publish. This form provides structure for consistency and transparency in reporting. For further information on Nature Portfolio policies, see our Editorial Policies and the Editorial Policy Checklist.

Statistics

For all statistical analyses, confirm that the following items are present in the figure legend, table legend, main text, or Methods section.

n/a	Confirmed	
☐	☒	The exact sample size (*n*) for each experimental group/condition, given as a discrete number and unit of measurement
☐	☒	A statement on whether measurements were taken from distinct samples or whether the same sample was measured repeatedly
☐	☒	The statistical test(s) used AND whether they are one- or two-sided *Only common tests should be described solely by name; describe more complex techniques in the Methods section.*
☐	☒	A description of all covariates tested
☐	☒	A description of any assumptions or corrections, such as tests of normality and adjustment for multiple comparisons
☐	☒	A full description of the statistical parameters including central tendency (e.g. means) or other basic estimates (e.g. regression coefficient) AND variation (e.g. standard deviation) or associated estimates of uncertainty (e.g. confidence intervals)
☐	☒	For null hypothesis testing, the test statistic (e.g. *F*, *t*, *r*) with confidence intervals, effect sizes, degrees of freedom and *P* value noted *Give P values as exact values whenever suitable.*
☒	☐	For Bayesian analysis, information on the choice of priors and Markov chain Monte Carlo settings
☒	☐	For hierarchical and complex designs, identification of the appropriate level for tests and full reporting of outcomes
☐	☒	Estimates of effect sizes (e.g. Cohen's *d*, Pearson's *r*), indicating how they were calculated

Our web collection on statistics for biologists contains articles on many of the points above.

Software and code

Policy information about availability of computer code

Data collection	MALDI imaging data were acquired on a timsTOF fleX instrument (Bruker) in negative Q-TOF ion mode at 10 µm pixel size. MRI images were acquired on a nanoScan PET/MRI (Mediso, Budapest, Hungary). Immunoblots were acquired with an Odyssey scanner (Licor) or Chemidoc MP imager (Biorad). Mass Spectrometry data were acquired with Thermo Scientific Xcalibur Version 4.1 and subsequent versions.
Data analysis	Targeted metabolomics analysis was performed using Tracefinderv4.1 (Thermo Scientific). Untargeted metabolomics analysis was performed using Compound Discoverer (Thermo Scientific v3.2). MALDI imaging analysis was performed using MetaboScape 2021b (Bruker) and ion distributions visualized with SCiLS Lab 2021c (Bruker). MRI imaging analysis was performed with VivoQuant ver4.0 (Invicro). Immunoblots images were analyses with Image Studio Lite 5.2 (Licor) and Chemidoc image lab 6.0 (Biorad). Mass spectrometry data were analyzed with Thermo Scientific Xcalibur Version 4.1 and subsequent versions. Immunohistochemistry images were visualized with Aperio ImageScope v12.4 (Leica Biosystems). The glutamine synthetatse protein structure (PDB 2QC8) was visualized with UCSF Chimera v1.15.

For manuscripts utilizing custom algorithms or software that are central to the research but not yet described in published literature, software must be made available to editors and reviewers. We strongly encourage code deposition in a community repository (e.g. GitHub). See the Nature Portfolio guidelines for submitting code & software for further information.

Data

Policy information about availability of data

All manuscripts must include a data availability statement. This statement should provide the following information, where applicable:

- Accession codes, unique identifiers, or web links for publicly available datasets
- A description of any restrictions on data availability
- For clinical datasets or third party data, please ensure that the statement adheres to our policy

All the data supporting the findings of this study are available within the article, and the supplementary information files. Source data file that support the findings of this study are stored at the Cancer Research UK Beatson Institute and are available from the corresponding author upon reasonable request. Requests for unique biological materials can be made to the corresponding author.

Field-specific reporting

Please select the one below that is the best fit for your research. If you are not sure, read the appropriate sections before making your selection.

☒ Life sciences ☐ Behavioural & social sciences ☐ Ecological, evolutionary & environmental sciences

For a reference copy of the document with all sections, see nature.com/documents/nr-reporting-summary-flat.pdf

Life sciences study design

All studies must disclose on these points even when the disclosure is negative.

Sample size	For animal experiments no statistic calculation was performed to predetermine the sample size. Sample size was chosen based on pilot experiments with small number of animals (n=2-4), or based on the outcome of similar experiments previously carried out at the same institution with similar murine models. For all other experiments no sample size calculation was performed, and sample sizes were chosen based on experience gained from previous studies.
Data exclusions	No data were excluded.
Replication	Multiple independent experiments were performed for cell culture-based studies as indicated in the figure legends. Tissue sections or fragments from at least 3 animals per genotype or condition were used for analysis, unless mentioned otherwise.
Randomization	Mice were randomly assigned to experimental groups taking into account their genotype and sex. For in vitro experiments group allocation was not relevant.
Blinding	Researchers were not blinded to genotype of animals reaching clinical endpoints at different stages for animal welfare reasons. The investigator(s) were blinded to genotype or treatment for MRI data analysis.

Reporting for specific materials, systems and methods

We require information from authors about some types of materials, experimental systems and methods used in many studies. Here, indicate whether each material, system or method listed is relevant to your study. If you are not sure if a list item applies to your research, read the appropriate section before selecting a response.

Materials & experimental systems

n/a	Involved in the study
☐	☒ Antibodies
☐	☒ Eukaryotic cell lines
☒	☐ Palaeontology and archaeology
☐	☒ Animals and other organisms
☒	☐ Human research participants
☒	☐ Clinical data
☒	☐ Dual use research of concern

Methods

n/a	Involved in the study
☒	☐ ChIP-seq
☒	☐ Flow cytometry
☒	☐ MRI-based neuroimaging

Antibodies

Antibodies used	Glutamine synthetase (HPA007316, Sigma-Aldrich), Glutamine synthetase (610517, BD Bioscience), Ornithine aminotransferase (ab137679, Abcam), β-actin (ab8229, Abcam), β-tubulin (T5201, Sigma-Aldrich), Vinculin (V9131, Sigma-Aldrich), anti-Rabbit-HRP (1:1000; 7074, Cell Signaling Technology), anti-Mouse-IRDye 800CW (1:2500; 926-32212, Licor), Anti-Goat-IRDye 680CW (1:2500; 926-68074, Licor).

Validation	The glutamine synthtetase antibodies were validated with cell and mouse models genetically engineered for GLUL in this study Fig 1c,d and 3h. All other antibodies used were validated for the species and applications used in this study (WB and IHC) as stated at the respective manufacturer's websites.

Eukaryotic cell lines

Policy information about cell lines

Cell line source(s)	HEK293 and HepG2 cell lines were obtained from ATCC. T16 cells are not commercially available and were previously characterized in Golebiewska et al. 2020;140(6):919-949. doi: 10.1007/s00401-020-02226-7.
Authentication	All cell lines were authenticated using Multiplex PCR-based STR analysis (Promega GenePrint 10 Kit, B9510, Promega)
Mycoplasma contamination	All cell lines tested negative for mycoplasma infection using the MycoAlert Mycoplasma Detection Kit (LT07-318, Lonza).
Commonly misidentified lines (See ICLAC register)	No commonly misidentified cell line was used in this study.

Animals and other organisms

Policy information about studies involving animals; ARRIVE guidelines recommended for reporting animal research

Laboratory animals	Mice with the following alleles Glul tm3Whla; Ctnnb1 lox(ex3); Rosa26DM.lsl-MYC; Trp53 tm1brn; K-rasLSL.G12D; Trp53R172H; Pdx-1-Cre were bred to obtain the allelic combiations indicated in the manuscript. Mice of both sexes aged eight weeks to 12 months, on a mixed background or backcrossed (N5-12) into a C57BL/6J background were used in this study. Mice were housed in University of Glasgow (UK) facilities, with the exception of germ-free mice housed at the Germ-free and Gnotobiotic Mouse facility at Ghent University, Belgium.
Wild animals	This study did not use wild animals.
Field-collected samples	This study did not use field collected samples.
Ethics oversight	Animal experiments were either subject to review by the University of Ghent Animal Ethics Committee or were performed in accordance with UK Home Office Regulations (project licences 70/8645 60/4181, PP6345023, PP0604995) and subject to review by the Animal Welfare and Ethical Review Board of the University of Glasgow.

Note that full information on the approval of the study protocol must also be provided in the manuscript.